FER-LIKE IRON DEFICIENCY-INDUCED TRANSCRIPTION FACTOR (FIT) accumulates in homo- and heterodimeric complexes in dynamic and inducible nuclear condensates associated with speckle components

Short title: FIT localizes in condensates

Ksenia Trofimov[1], Regina Gratz[1,§], Rumen Ivanov[1], Yvonne Stahl[2,3], Petra Bauer[1,3,*], Tzvetina Brumbarova[1,*]

[1] Institute of Botany, Heinrich-Heine-University, 40225 Düsseldorf, Germany
[2] Institute for Developmental Genetics, Heinrich-Heine-University, 40225 Düsseldorf, Germany
[3] Cluster of Excellence on Plant Science (CEPLAS), Heinrich-Heine-University, 40225 Düsseldorf, Germany
***** Shared corresponding authors: Tzvetina Brumbarova (Tzvetina.Brumbarova@hhu.de), Petra Bauer (Petra.Bauer@hhu.de)
§ Present address: Umeå Plant Science Centre (*UPSC*), Department of Forest Genetics and Plant Physiology, Swedish University of Agricultural Sciences, 90183 Umeå, Sweden

The author responsible for distribution of materials integral to the findings presented in this article in accordance with the policy described in the Instructions for Authors (https://academic.oup.com/plcell/pages/General-Instructions) is: Petra Bauer (Petra.Bauer@hhu.de).

Highlights

- FIT undergoes light-induced condensation and localizes to NBs, likely via LLPS
- Functionally relevant Ser271/272 defines an intrinsically disordered region and influences NB formation dynamics
- NBs are preferential sites for FIT dimerization with FIT and bHLH039, dependent on Ser271/272
- FIT NBs colocalize with NB markers related to splicing and light signalling

Keywords

29 anisotropy, bHLH039, condensates, FIT, FRAP, FRET-FLIM, IDR, LLPS, nuclear body,
30 photobody, speckle, SR45

Abbreviations

bHLH	basic helix-loop-helix
bHLH039	BASIC HELIX-LOOP-HELIX039
C	mCherry
FIT	FER-LIKE IRON DEFICIENCY-INDUCED TRANSCRIPTION FACTOR
FLIM	fluorescence lifetime imaging microscopy
FRAP	fluorescence recovery after photobleaching
FRET	fluorescence resonance energy transfer
G	GFP
GFP	GREEN FLUORESCENT PROTEIN
IDR	intrinsically disordered region
LLPS	liquid-liquid phase separation
mCherry	monomeric Cherry
mRFP	monomeric RED FLUORESCENT PROTEIN
NB	nuclear body
NP	nucleoplasm
PB	photobody
R	mRFP
TF	transcription factor

Abstract

Several nuclear proteins undergo condensation. The question remains often whether this property is coupled to a functional aspect of the protein in the nucleus. The basic helix-loop-helix (bHLH) FER-LIKE IRON DEFICIENCY-INDUCED TRANSCRIPTION FACTOR (FIT) integrates internal and external signals to control the amount of iron that is acquired in accordance with growth. The previously described C-terminal Ser271/272 allows FIT to form active complexes with subgroup Ib bHLH factors such as bHLH039. FIT has lower nuclear mobility than mutant FITmSS271AA, but this behavior has remained mechanistically and functionally obscure. Here, we show that FIT undergoes a light-inducible subnuclear partitioning into nuclear condensates that we termed FIT nuclear bodies (NBs). The characteristics of FIT NBs could be examined using a standardized FIT NB analysis procedure coupled with different types of quantitative and qualitative microscopy-based approaches. We found that FIT condensates were likely formed by liquid-liquid phase separation. FIT accumulated preferentially in FIT NBs versus nucleoplasm when engaged in protein complexes with itself and with bHLH039. FITmSS271AA, instead, localized to NBs with different dynamics. FIT colocalized with splicing and light signaling NB markers. Hence, the inducible highly dynamic FIT condensates link active transcription factor complexes with posttranscriptional regulation processes.

Introduction

As sessile organisms, plants must adjust to an ever-changing environment. Read-out of environmental cues and rapid acclimation are necessary to ensure the plant's vitality. Accordingly, plants control micronutrient uptake. Overaccumulation causes toxicity but lack of a micronutrient leads to deficiency symptoms. Even though iron is one of the most abundant elements in the soil, its bioavailability as micronutrient is limited in most soils, rendering iron uptake a challenge for plants (Römheld and Marschner, 1986; Wedepohl, 1995).

An essential regulatory protein needed for iron acquisition is the basic helix-loop-helix (bHLH) transcription factor (TF) FER-LIKE IRON DEFICIENCY-INDUCED TRANSCRIPTION FACTOR (FIT; Colangelo and Guerinot, 2004; Jakoby et al., 2004; Yuan et al., 2005; Bauer et al., 2007). FIT is activated upon iron deficiency downstream of a cascade of bHLH TFs (Zhang et al., 2015; Li et al., 2016; Liang et al., 2017; Kim et al., 2019; Gao et al., 2020) and of a calcium-sensing protein kinase able to target phosphorylation site Ser271/272 of FIT (Gratz et al., 2019). FIT alone is not sufficient to upregulate iron acquisition, while it is active in a heterodimeric complex together with a member of the bHLH subgroup Ib such as bHLH039 (Yuan et al., 2008; Wang et al., 2013). Furthermore, FIT action is regulated through protein-protein contacts with multiple key players of hormonal and abiotic stress signaling pathways (Lingam et al., 2011; Le et al., 2016; Wild et al., 2016; Cui et al., 2018; Gratz et al., 2019, 2020). Thus, FIT behaves as a regulatory hub in root cells that perceives external and internal cues to adjust iron acquisition with growth (Schwarz and Bauer, 2020; Kanwar et al., 2021).

The subcellular localization of the FIT-bHLH039 module is remarkable. bHLH039 alone is inactive and present mainly close to the plasma membrane in cytoplasmic foci, while bHLH039 together with FIT localizes in the nucleus (Trofimov et al., 2019). FIT is predominately localized in the nucleus but not as mobile compared to mutant FITmSS271AA, that is a less active mutant form of FIT (Gratz et al., 2019). Subcellular partitioning of proteins involved in nutrient uptake has until now not been enough in the focus of research to understand the significance of the differing subcellular localization patterns.

One prominent type of subnuclear partitioning is conferred by biomolecular condensates, or nuclear bodies (NBs). NBs are membraneless, nuclear subcompartments, which can be of stable or dynamic nature. To form condensates,

proteins need to have particular features that enable protein interactions and compaction in three-dimensional space. IDRs are flexible protein regions that allow conformational changes, and thus various interactions, leading to the required multivalency of a protein for condensate formation (Tarczewska and Greb-Markiewicz, 2019; Emenecker et al., 2020). As Arabidopsis TFs are enriched in IDRs (Strader et al., 2022) it is not unlikely that the resulting multivalency in TFs drives condensation and results in microenvironments for interaction, probably more often than so far studied. IDRs are particularly characteristic in bHLH TFs in vertebrates and invertebrates (Tarczewska and Greb-Markiewicz, 2019), suggesting that this feature may also be relevant for the bHLH TFs of plants. One possibility for condensates to form is to undergo liquid-liquid phase separation (LLPS). In this process, a solution is demixed into two or more phases (Emenecker et al., 2020). This mechanism has been examined in simplified *in vitro* systems, but the involvement of different cell components renders the mechanism more complex *in vivo* (Fang et al., 2019; Riback et al., 2020; Zhu et al., 2021).

NBs comprise an immense variety of types, and plants and animals share several of them, e.g. the nucleolus, Cajal bodies, and speckles. The nucleolus is involved in transcription of ribosomal DNA, processing of ribosomal RNA, and ribosome biogenesis (Kalinina et al., 2018; Lafontaine et al., 2021). Nucleoli share components and function with Cajal bodies, which are e.g. ribonucleoproteins and RNA processing (Love et al., 2017; Trinkle-Mulcahy and Sleeman, 2017). Speckles are known spliceosomal sites (Reddy et al., 2012; Galganski et al., 2017). Plant-specific NBs are photobodies (PBs), which are triggered by light, temperature, and circadian clock (Pardi and Nusinow, 2021). PBs harbor regulatory complexes of the photomorphogenic responses, including photoreceptors like phytochromes (phy) and bHLH TFs belonging to the PHYTOCHROME INTERACTING FACTORs (PIFs; Pardi and Nusinow, 2021). Another trigger for inducible condensate formation is temperature (Jung et al., 2020; Zhu et al., 2021).

NBs may act as hubs integrating environmental signals (Emenecker et al., 2020; Meyer, 2020). Especially PBs may combine external cues, such as light, as an input signal to steer developmental processes (Kaiserli et al., 2015; Meyer, 2020; Pardi and Nusinow, 2021). It is proposed that the formation of NBs could be an ancient mechanism for spatial organization within the nucleus (Emenecker et al., 2020). As more evidence on

condensation in plants arises, this topic remains barely examined in the scope of plant nutrition.

The motivation for our study was to elucidate the mechanism behind subcellular distribution and nuclear mobility of FIT. We had found an interesting hint that FIT may undergo light-inducible nuclear condensation, when we detected FIT nuclear bodies (NBs). We developed a standardized FIT NB analysis procedure and applied it to characterize quantitative and qualitative aspects of the dynamic NB formation using different microscopy-based techniques. Thereby, we were able to link FIT NB formation with the activity status of FIT to form functional protein complexes. We found that splicing and light signaling were also associated with FIT NBs. Thus, this study lays ground for FIT NBs being regulatory hubs steering nutritional signalling, and associating functional significance to FIT protein condensate formation.

Results

FIT localizes to NBs in light-inducible and dynamic manner likely as a result of LLPS

The TF FIT has a dynamic mobility and capacity to form TF complexes inside plant cells (Gratz et al., 2019; Trofimov et al., 2019). To explore possible mechanisms for dynamic FIT subcellular localization, we performed a microscopic study on FIT-GFP protein localization in the root epidermis of the root differentiation zone of 5-d-old iron-deficient seedlings of *Arabidopsis thaliana* (Arabidopsis), where FIT is active and iron acquisition occurs ($35S_{pro}$:FIT-GFP complemented *fit-3*; Jakoby et al., 2004; Gratz et al., 2019). At first microscopic inspection, FIT-GFP was evenly distributed within the nucleus. After a lag time, FIT-GFP became re-localized at the subnuclear level (**Figure 1A**). Discrete FIT-GFP nuclear spots were visible after 40 min earliest, sometimes taking up to 2 h to appear. One to four spots were observed per nucleus. Nuclear FIT-GFP spots were triggered by exposure of whole seedlings to 488 nm laser for several minutes. The observation of FIT nuclear spots in the root epidermis of the root differentiation zone was very interesting, suggesting that these might perhaps be NBs containing FIT. However, further inspection of the nuclear spots in root cells in this differentiating root zone was hampered by several difficulties, namely the small size and low accessibility of the nucleus, comparably low level of expression of FIT in roots (see also Lingam et al., 2011; Meiser et al., 2011), and especially considering the long lag time for detecting the nuclear spots. These factors made it impossible for us to apply quantitative fluorescence

microscopy techniques to draw validated conclusions on the nature, dynamics, and functional significance of nuclear spots in root epidermis cells of the root differentiation zone of iron-deficient seedlings.

FIT-GFP that was transiently expressed in *Nicotiana benthamiana* (*N. benthamiana*) leaf epidermis cells under a β-estradiol-inducible promoter to control protein expression showed a very similar re-localization of FIT-GFP into nuclear spots as observed in the Arabidopsis root epidermis, again triggered by treatment with a 488 nm laser light stimulus. Differences were, however, the duration of the lag time needed to observe this phenomenon, and the number of nuclear spots. As in Arabidopsis, FIT-GFP localized initially in uniform manner to the entire nucleus (t=0) of *N. benthamiana* leaf epidermis cells. A short duration of 1 min 488 nm laser light excitation induced the formation of FIT-GFP signals in discrete spots inside the nucleus after a lag time of only five minutes (t=5; **Figure 1B and Supplemental Movie S1A**). The nuclear FIT spots were systematically initiated, and nearly all nuclei in the imaged leaf disk showed numerous spots. A similar laser light excitation procedure was previously found to elicit PB formation of cryptochrome2 (CRY2) in Arabidopsis protoplasts and HEK293T cells (Wang et al., 2021). We deduced that the spots of FIT-GFP signal were NBs. FIT NB formation was not dependent on the fluorescent tag, as it was similar for FIT-mCherry when co-excited with 488 nm laser light (**Figure 1C**). Another TF and interactor of FIT, ZINC FINGER OF ARABIDOPSIS THALIANA12-GFP (ZAT12-GFP; Le et al., 2016), did not localize to NBs under the same imaging conditions (**Figure 1D and Supplemental Movie S1B**). Therefore, we concluded that FIT localization to NBs was a specificity of FIT and that formation of FIT NBs was not artificially caused by fluorescent tags or the imaging setup. Importantly, the *N. benthamiana* epidermis expression system was suited to control the parameters for light-induced triggering of FIT NBs and their quantitative analysis by fluorescence microscopy. We then developed a standardized experimental procedure for qualitative and quantitative FIT NB analysis in *N. benthamiana* (hereafter named 'standardized FIT NB analysis procedure'; **Supplemental Figure S1**).

Liquid-liquid phase separation (LLPS) is a possible way for condensate formation, and liquid-like features are quantifiable by mobility and shape analysis within condensates (Shin et al., 2017; Wang et al., 2021). We used the standardized FIT NB analysis procedure to examine whether this could also be a mechanism underlying the FIT NB formation. Mobility of FIT NBs was tested with the fluorescence recovery after

199 photobleaching (FRAP) approach (Bancaud et al., 2010; Trofimov et al., 2019) by
200 recording the recovery of the fluorescence intensity over time in a bleached NB
201 (**Figure 1E-G**). According to relative fluorescence intensity the fluorescence signal
202 recovered to a high extent with FIT NBs (**Figure 1F**), and the calculated mobile fraction
203 of the NB protein was on average 80% (**Figure 1G**). Shape analysis of FIT NBs showed
204 that the NBs reached a high circularity score (**Figure 1H**). According to Wang et al. (2021),
205 fluorescence recovery and circularity scores as the ones measured for FIT NBs reflect
206 high mobility and circular shape. Thus, FIT NBs behave in a liquid-like manner suggesting
207 that LLPS might be the mechanism leading to FIT NB formation.
208 In summary, the developed standardized FIT NB analysis procedure was well
209 suited for investigating dynamic properties of light-induced FIT NBs and characterizing
210 them as the likely result of LLPS. Because of these properties, it is justified to term them
211 'FIT NBs'. We hypothesized that NB formation is a feature of the FIT protein that provides
212 regulatory specificity, and we subsequently investigated this hypothesis using the
213 developed standardized FIT NB analysis procedure in all subsequent assays below.

214 **FIT forms homodimeric complexes preferentially in NBs, dependent on Ser271/272**
215 Next, we asked which properties of the FIT protein enable NB formation. Residue
216 Ser271/272 is important for the homo- and heterodimerization capacity of FIT (Gratz et
217 al., 2019). We therefore asked whether this site has an influence on FIT NB formation,
218 and we compared the ability for NB formation of mutant FITmSS271AA-GFP with that of
219 wild-type FIT-GFP protein.
220 FITmSS271AA-GFP also localized to NBs, however with different dynamics. The
221 formation of FITmSS271AA NBs was delayed in time (**Figure 2A**; t=15 instead of t=5).
222 While FIT-GFP NB formation started in the first minutes after excitation (**Supplemental**
223 **Movie S1A**), FITmSS271AA-GFP NB formation occurred earliest 10 min after excitation
224 (**Supplemental Movie S1C**). In addition, NB number and size of FITmSS271AA-GFP
225 were decreased in comparison to the ones from wild-type FIT-GFP (**Figure 2, B and C**).
226 Hence, the dynamics of NB formation were dependent on Ser271/272.
227 The process of condensation is facilitated when proteins possess IDRs, since,
228 importantly, IDRs may engage in numerous interactions in space due to rapid
229 conformational changes (Tarczewska and Greb-Markiewicz, 2019; Emenecker et al.,
230 2020). The three-dimensional conformation of wild-type FIT had predicted stretches of

intrinsic disorganization, peaking before and at the basic region of the bHLH domain, and two in the C-terminal part, one of them around the Ser271/272 site (termed IDR$^{Ser271/272}$; **Supplemental Figure S2A**). In contrast, in the FITmSS271AA mutant this C-terminal region was no longer classified as IDR (**Supplemental Figure S2B**). This underlined the significance of the Ser271/272 site, not only for interaction but also for FIT NB formation.

We then tested whether FIT homodimerization was preferentially associated with NB formation. For that, we investigated whether FIT-GFP shows a differentiated homodimerization strength, first, inside the NBs versus the nucleoplasm (NP), and second, as wild-type FIT versus the mutant FITmSS271AA-GFP protein by performing anisotropy (or homo-FRET) measurements. Energy transfer between the same kind of fluorescently tagged proteins leads to depolarization of the emitted light (Stahl et al., 2013; Weidtkamp-Peters et al., 2022). Fluorescence anisotropy (FA) describes this depolarization and gives hints on the dimerization and oligomerization status of a protein as the FA value decreases (**Figure 3A**). We measured FA before (t=0) and after NB formation (t=5 for FIT and t=15 for FITmSS271AA), and analyzed the homodimerization strength for the whole nucleus, the NBs, and the residual NP (**Figure 3B-D**). Free GFP and GFP-GFP constructs were used as references for monomers and dimers (**Figure 3C and D**).

Whole nucleus FA values were lower at t=5 than at t=0 for FIT-GFP. Additionally, FA values were lower within the NBs compared to the NP (**Figure 3C**). Compared to wild-type FIT-GFP, FA values were not reduced for mutant FITmSS271AA-GFP at t=15 compared to t=0. Also, the FA values did not differ between NBs and NP for the mutant protein (**Figure 3D**). This indicated the presence of homodimeric FIT complexes in NBs.

In summary, wild-type FIT had better capacities to localize to NBs than mutant FITmSS271AA, presumably due its IDR$^{Ser271/272}$ at the C-terminus. NBs were nuclear sites in which FIT formed preferentially homodimeric protein complexes.

FIT-bHLH039 interaction complexes preferentially accumulate in FIT NBs

FIT engages in protein-protein interactions with bHLH039 to steer iron uptake target gene induction in the nucleus, while mutant FITmSS271AA protein is less active in interacting with bHLH039 (Gratz et al., 2019). Hence, we tested whether FIT also interacts with bHLH039 preferentially inside NBs and whether mutant FITmSS271AA differs in this ability from wild-type FIT protein. bHLH039 alone does not localize inside the nucleus but

requires FIT for nuclear localization (Trofimov et al., 2019), so that bHLH039 was not used alone to test its subnuclear localization.

Upon co-expression, FIT-GFP and bHLH039-mCherry colocalized fully in NBs that resembled the previously described FIT NBs. In the beginning, both proteins were uniformly distributed within the nucleus (t=0), and later became localized in NBs (t=5; **Figure 4A**).

We then examined the heterodimerization strength of FIT-GFP and bHLH039-mCherry, and FITmSS271AA-GFP and bHLH039-mCherry by FRET-fluorescence lifetime imaging microscopy (FRET-FLIM) measurements. In case of protein interaction (close proximity, ≤10 nm), energy transfer between a fluorescently tagged donor and a fluorescently tagged acceptor decreases the fluorescence lifetime of the donor (**Figure 4B;** Borst and Visser, 2010; Weidtkamp-Peters and Stahl, 2017). We quantified the fluorescence lifetime of FIT-GFP and FITmSS271AA-GFP respective of heterodimerization before (t=0) and after NB formation (t=5 for FIT and t=15 for FITmSS271AA) in the whole nucleus, in NBs, and in the NP (**Figure 4C-E**). FIT-GFP and FITmSS271AA-GFP (donor only) served as negative controls.

Fluorescence lifetime was decreased for the pair FIT-GFP and bHLH039-mCherry at t=5 within NBs compared to all other measured areas (**Figure 4D**). In contrast to that, the fluorescence lifetime decrease for the pair FITmSS271AA-GFP and bHLH039-mCherry at t=15 was not different between NBs and NP (**Figure 4E**). This indicated that heterodimeric complexes accumulated preferentially in FIT NBs.

In summary, heterodimerization of FIT with bHLH039 was spatially concentrated in NBs versus the remaining nuclear space and was less prominent for FITmSS271AA. Hence, the capacity of FIT to form an active TF complex was coupled with its presence in NBs. The occurrence of FIT homo- and heterodimerization preferentially in NBs suggests that FIT protein interaction may drive condensation. We therefore concluded that FIT NBs may be sites with active TF complexes for iron deficiency response regulation.

FIT NBs colocalize with speckle components

Numerous NB types are known, and they are associated with particular proteins that are indicative of the NB type. To further understand the identity, dynamics, and function of FIT NBs, we co-expressed FIT-GFP with seven different NB markers from The Plant Nuclear Marker collection (NASC) and observed NB formation and protein

colocalization before (t=0) and after FIT NB formation (t=5). In cases where we detected a colocalization with FIT-GFP, we analyzed the localization of NB markers also in the single expression at t=0 and at t=5 after the 488 nm excitation, to detect potentially different patterns in single and co-expression.

All seven NB markers were expressed together with FIT-GFP, and according to the resulting extent of colocalization we subdivided them into three different types. The first type (type I) did not colocalize with FIT-GFP neither at t=0 nor at t=5. This was the case for the Cajal body markers coilin-mRFP and U2 snRNP-specific protein U2B"-mRFP (**Supplemental Figure S3**; Lorković et al., 2004; Collier et al., 2006). Coilin-mRFP localized into a NB within and around the nucleolus (**Supplemental Figure S3A**). The NBs of U2B"-mRFP were also close to the nucleolus (**Supplemental Figure S3B**). Hence, FIT-GFP was not associated with Cajal bodies.

The second type (type II) of NB markers were partially colocalized with FIT-GFP. This included the speckle components ARGININE/SERINE-RICH45-mRFP (SR45) and the serine/arginine-rich matrix protein SRm102-mRFP. SR45 is involved in splicing and alternative splicing and is part of the spliceosome in speckles (Ali et al., 2003), and was recently found to be involved in splicing of iron homeostasis genes (Fanara et al., 2022). SRm102 is a speckle component (Kim et al., 2016). SR45-mRFP localized barely in the NP but inside few and very large NBs that remained constant at t=0 and t=5. FIT-GFP did not colocalize in those NBs at t=0, however, it colocalized with the large SR45-mRFP NBs at t=5 (**Figure 5A**). FIT-GFP also localized in typical FIT NBs in the residual NP at t=5 (**Figure 5A**). SRm102-mRFP showed low expression in the NP and stronger expression in a few NBs that also remained constant at t=0 and t=5. FIT-GFP colocalized with SRm102-mRFP in only few instances at t=5, but not t=0, while most FIT NBs did not colocalize with SRm102-mRFP NBs (**Figure 5B**). Both SR45-mRFP and SRm102-mRFP had the same localization pattern at t=0 and t=5, irrespective of FIT-GFP co-expression or 488 nm excitation (**Supplemental Figure S4**). These type II NB markers seemed to recruit FIT-GFP into NBs after 488 nm excitation that were present (pre-existing) before FIT-GFP NB formation, while FIT-GFP localized additionally in separate FIT NBs. Hence, FIT became associated with splicing components and speckles upon the light trigger.

A third type (type III) of three NBs markers, namely UAP56H2-mRFP, P15H1-mRFP, and PININ-mRFP, were fully colocalized with FIT-GFP. Until now, these NB marker proteins are not well described in plants. UAP56H2 is a RNA helicase, which is

involved in mRNA export (Kammel et al., 2013). P15H1 was found as a putative Arabidopsis orthologue of an exon junction complex component in humans (Pendle et al., 2005), while PININ has a redundant role to its paralogue apoptotic chromatin condensation inducer in the nucleus (ACINUS) in alternative splicing (Bi et al., 2021). UAP56H2-mRFP and P15H1-mRFP did not localize in NBs and were not responsive to the 488 nm excitation when expressed alone or together with FIT-GFP at t=0 (**Figure 6, A and B and Supplemental Figure S4, C and D**). When co-expressed with FIT-GFP and following the 488 nm excitation, at t=5, the two NB markers adopted the FIT NB pattern and colocalized with FIT-GFP in FIT NBs (**Figure 6, A and B**). PININ-mRFP was also uniformly distributed in the nucleus at t=0 like FIT-GFP and fully colocalized with FIT NBs at t=5 (**Figure 6C**). But curiously, PININ-mRFP showed a very different localization in the single expression. Predominately, it localized to a very large NB besides several small NBs with no expression in the NP at t=0 and at t=5 (**Supplemental Figure S4E**). Thus, FIT-GFP recruited these type III NB marker and speckle proteins fully into FIT NBs. Since type III NB markers are also potentially involved in splicing and mRNA export from the nucleus, these same functions may be relevant in FIT NBs.

Taken together, the colocalization studies underlined the dynamic behavior of inducible FIT NB formation. FIT NBs had a speckle function, in which on the one hand FIT was recruited itself into pre-existing splicing-related NBs (SR45-mRFP and SRm102-mRFP, type II), while on the other hand it also recruited speckle-localized proteins into FIT NBs (UAP56H2-mRFP, P15H1-mRFP, and PININ-mRFP, type III).

PB components influence FIT NB localization and formation

PBs are plant-specific condensates which harbor various light signaling components (Kircher et al., 2002; Bauer et al., 2004). Among them are the bHLH TFs of the PIF family. As key regulators of photomorphogenesis, they integrate light signals in various developmental and physiological response pathways (Leivar and Monte, 2014; Pham et al., 2018). Indeed, PIF4 may control iron responses in Arabidopsis based on computational analysis of iron deficiency response gene expression networks (Brumbarova and Ivanov, 2019). We tested in the same manner as described above for NB markers, whether FIT NBs coincide with two of the described PB markers, PIF3-mCherry and PIF4-mCherry (Van Buskirk et al., 2014; Qiu et al., 2019, 2021).

We detected distinct localization patterns for PIF3-mCherry and PIF4-mCherry. At t=0, PIF3-mCherry was predominantly localized in a single large PB (**Figure 7A**). In general, localization of single expressed PIF3-mCherry remained unchanged at t=0 and t=15 (**Supplemental Figure S5A**). Upon co-expression, FIT-GFP was initially not present in PIF3-mCherry PB at t=0. After 488 nm excitation and at t=5, FIT NBs were still not visible. Instead, FIT-GFP accumulated and finally colocalized with the large PIF3-mCherry PB at t=15, while the typical FIT NBs did not appear (**Figure 7A**).

PIF4-mCherry localized in two different patterns, and both differed substantially from that of PIF3-mCherry. In the one pattern at t=0, PIF4-mCherry was not localized to any PBs, but instead was uniformly distributed in the NP as was the case for FIT-GFP. Such a pattern was also seen at t=15, and then neither PIF4-mCherry nor FIT-GFP were localized in any PBs/NBs (**Figure 7B**). In the other pattern, PIF4-mCherry and FIT-GFP localized in multiple PBs at t=0 and t=15, whereas none of them corresponded morphologically to the typical FIT NBs (**Figure 7C**). The same two localization patterns were also found for PIF4-mCherry in the single expression, whereby 488 nm excitation did not alter PIF4-mCherry localization (**Supplemental Figure S5, B and C**).

Hence, FIT was able to localize to PBs when co-expressed with PIF3 and PIF4, raising the possibility that FIT is a key regulator to cross-connect iron acquisition regulation and light signaling pathways.

Discussion

In this study, we uncovered a previously unknown phenomenon, the light-induced accumulation of FIT condensates in FIT NBs. LLPS was most likely the underlying mechanism for this highly dynamic process. FIT NBs were enriched in active FIT TF complexes for iron deficiency gene regulation. FIT associated with speckles and PBs in a highly dynamic fashion. Based on these data, FIT NBs are dynamic microenvironments with active FIT TF complexes that possibly are hubs to cross connect transcriptional iron deficiency gene expression with post-transcriptional regulation and light signaling.

A standardized procedure for FIT NB induction was crucial to delineate the characteristics of FIT NBs in reliable manner

A major aim of this study was to characterize the nature and potential function of light-induced FIT NBs. To be able to apply the quantitative microscopy-based techniques, we needed to control the appearance of NBs in reliable manner and FIT-GFP fluorescence

needed to be sufficiently strong. This was clearly a limitation for inspection of root epidermis cells of the root differentiation zone in iron-deficient plants in which FIT-controlled iron uptake takes place. Not every root epidermis cell showed NBs and only few FIT NBs were detectable after a delay of 40 min to 2 h. Since condensation depleted FIT protein in the nucleoplasm, the remaining low FIT protein concentration can be the reason why FIT NBs remained few in number in the Arabidopsis root cells. The *N. benthamiana* protein expression system did not present these limitations and high-quality measurement data were obtained for all experimental series. Furthermore, this expression system is a well-established and widely utilized system in plant biology (Martin et al., 2009; Bleckmann et al., 2010; Leonelli et al., 2016; Burkart et al., 2022). The developed standardized assay generated reliable and accurate data for statistical analysis and quantification to conclude about FIT NB characteristics.

Condensation likely explains the reduced mobility of FIT-GFP versus FITmSS271AA-GFP seen in a previous study (Gratz et al., 2019). In liquid state, condensates are still more mobile than in the solid one. According to FRAP data, FIT NBs maintained a dynamic exchange of FIT protein with the surrounding NP. FIT NBs were also mostly of circular shape. Circular condensates appear as droplets, in contrast to solid-like condensates that are irregularly shaped (Shin et al., 2017). These two characteristics speak in favour of liquid-like features, suggesting that LLPS underlies FIT NB formation. A similar situation was described for CRY2 PBs, which were also of circular shape with mobile protein inside PBs (Wang et al., 2021). bHLH039 was found accumulated in cytoplasmic foci at the cell periphery (Trofimov et al., 2019). In such foci, bHLH039 was immobile, and we suspect it was in a non-functional state in the absence of FIT. This underlines the understanding that liquid condensates such as FIT NBs are dynamic microenvironments, whereas immobile condensates point rather towards a solid and pathological state (Shin et al., 2017).

In conclusion, the properties of liquid condensation along with the findings that it occurred irrespective of the fluorescence protein tag preferentially with wild-type FIT, but with different dynamics for the mutant FITmSS271AA and not at all for ZAT12, allowed us to coin the term of ‘FIT NBs’.

IDR$^{Ser271/272}$ was crucial for interaction and NB formation of FIT

FIT NBs were hotspots for FIT interaction, allowing to assume that they are integrated in the iron deficiency response as interaction hubs. FIT formed homodimers and heterodimers with bHLH039 preferentially in NBs compared with the NP. These abilities distinguished wild-type FIT and mutant FITmSS271AA. According to these findings FITmSS271AA was less successful in interacting within NBs, indicating that wild-type FIT is a multivalent protein and IDR$^{Ser271/272}$ is important for that. bHLH proteins interact with other proteins via the helix-loop-helix interface, which may certainly also be the case for FIT. Our study supports previous reports that FIT protein interaction via its C-terminus is relevant (Lingam et al., 2011; Le et al., 2016; Gratz et al., 2019). The property of being able to interact via the HLH and via the C-terminal domain allows FIT to be multivalent. It could not be distinguished whether FIT homodimers were a prerequisite for the localization of bHLH039 in NBs or whether FIT-bHLH039 complexes also initiated NBs on their own.

The predicted C-terminal FIT IDR$^{Ser271/272}$ was relevant for NB formation capacity. IDRs are often required for protein interactions of hub proteins since the flexible IDRs adapt to interactions with multiple protein partners and are therefore crucial for multivalency (Tarczewska and Greb-Markiewicz, 2019; Emenecker et al., 2020; Salladini et al., 2020). Besides, evidence exists that the amino acid composition of IDRs is crucial for condensation (Powers et al., 2019; Emenecker et al., 2021; Huang et al., 2022). Very interestingly, posttranslational modification in form of phosphorylation within IDRs is suggested to be a mechanism to regulate condensate formation (Owen and Shewmaker, 2019). Ser271/272 is targeted by a FIT-interacting protein kinase that was shown to affect FIT activity *in vivo* and FIT phosphorylation *in vitro* (Gratz et al., 2019). Hence, phosphorylation of Ser271/272 might perhaps be a trigger for NB formation *in vivo*.

Formation of FIT NB could happen *de novo* but also associate with pre-existing condensates in the nucleus

FIT may have formed FIT NBs as entirely newly formed structures upon the light trigger. But it is also possible that FIT joined pre-existing NBs, which then became the structures we termed FIT NBs. Partial or full colocalization of FIT-GFP with NB and PB markers revealed the remarkably high and intriguing dynamic nature of FIT NBs and suggests that both possibilities are plausible. FIT NBs are light-triggered, and this speaks

in favor of pre-existing NBs. Since FIT does not possess light-responsive domains, it is most likely that a light-responsive protein must be inducing FIT NB formation. The basic leucine zipper TF ELONGATED HYPOCOTYL5 (HY5) could be a good candidate, since HY5 is a mobile protein involved in iron acquisition in tomato (Gao et al., 2021; Guo et al., 2021). Possibly activation and condensation involve not only the studied NB and PB markers but also potentially signaling proteins or further scaffold proteins that are part of the multivalent protein complexes in FIT NBs. On the other hand, FIT-GFP accumulated not only in FIT NBs but also in the pre-existing NBs with type II NB markers (SR45 and SRm102) after the FIT NB induction procedure. In this respect, type II markers were similar to PIF3 and PIF4. FIT-GFP was recruited to pre-existing PBs and again only after the light trigger. Interestingly, typical FIT NB formation did not occur in the presence of PB markers, indicating that they must have had a strong effect on recruiting FIT. Overall, the dynamics of FIT colocalization with type II NB and PB markers suggest that these condensates dictated FIT condensation in their own pre-existing NBs/PBs. This recruiting process could be navigated via protein-protein interaction since this is the driving force of condensation (Kaiserli et al., 2015; Emenecker et al., 2020).

Speaking in favor of a *de novo* FIT NB formation is the localization with type III NB markers. The three fully colocalizing type III NB markers (UAP56H2, P15H1 and PININ) accumulated only in FIT NBs upon co-expression with FIT and mostly not on their own. The same was true for bHLH039, that joined FIT in FIT NBs, showing that FIT not only facilitated bHLH039 nuclear localization (Trofimov et al., 2019) but also condensation. Interestingly, FIT was able to change PININ nuclear localization. In single expression, PININ was localized to a major large NB, but in colocalization with FIT it joined the typical FIT NBs. This suggests that FIT dictates bHLH039 and type III NB markers and highlights that FIT is also able to set the tone for NB formation. Hence, FIT can recruit other proteins into NBs, and it is possible that FIT forms its own NBs. Protein-protein interaction could underly this recruitment, as evident for bHLH039 (Kaiserli et al., 2015; Emenecker et al., 2020). Ultimately, as a high diversification of condensates exists, a combination of newly formed NBs and localization to pre-existing NBs cannot be ruled out. Given the variety of proteins localizing in condensates, effort in isolating FIT NBs and identification of proteins within FIT NBs is necessary to further uncover the driving forces of FIT NB formation.

FIT NBs might have a transcriptional and post-transcriptional function

Since the type II and III markers are splicing components, the colocalization studies suggest that FIT NBs are speckles. On the one hand, the speckle nature coincides well with the dynamic nature of FIT NBs. Like FIT NBs, speckles are highly dynamic. They are forming around transcriptionally active sites in the interchromatin regions recruiting several protein functions like mRNA synthesis, maturation, splicing and export (Reddy et al., 2012; Galganski et al., 2017). The type II speckle component SR45, for instance, was shown to be a highly mobile protein in speckles and required phosphorylation for proper speckle localization (Ali et al., 2003; Reddy et al., 2012). These processes fit well to the described FIT NB attributes. On the other hand, speckle components are also linked with epigenetic mechanisms (Mikulski et al., 2022). The characterization of FIT NBs as speckles is interesting because regulation of splicing and epigenetic regulation is associated with iron deficiency gene expression. Genes were spliced incorrectly in a *sr45-1* null mutant Arabidopsis line, and gene expression of *FIT* and FIT target genes was increased in *sr45-1* seedlings, showing that an interplay between SR45 and the iron uptake machinery exists (Fanara et al., 2022). Alternative splicing was detected for FIT targets and the *BHLH* subgroup Ib genes in iron-deficient versus iron-sufficient conditions (Li et al., 2013). Hence, FIT NBs may regulate iron uptake gene expression at posttranscriptional level. Notably, PININ (type III), together with ACINUS, were shown to stabilize SR45 (type II) in plants (Bi et al., 2021). Further, UAP56H2, P15H1, and PININ (type III) are connected to SR45 and SRm102 (type II) in mammalian cells as all being part of the exon junction complex and interacting with each other (Lin et al., 2004; Pendle et al., 2005). This is an interesting parallel, as it suggests that type II and type III marker localization is conserved across kingdoms, underlying the ancient nature of condensates. Indeed, SR45 and PININ located to a very large NB in non-induced cells. This opens the possibility that the two proteins might localize to the same speckle, as also might FIT. Taken together, the observations confirm the high diversification and complexity of FIT NBs and speckles (Lorković et al., 2008) and it is tempting to speculate that FIT might regulate splicing and alternative splicing of its target genes by recruiting speckle components.

FIT is itself a direct target of FIT and the FIT-bHLH039 complex (Wang et al., 2007; Naranjo-Arcos et al., 2017), and perhaps FIT NB speckles appear at the *FIT* transcription site. Indeed, coupling of transcription with splicing or alternative splicing is an established

idea in the mammalian field, and evidence for co-transcriptional splicing in plants is also recently rising (Nojima et al., 2015; Zhu et al., 2018; Chaudhary et al., 2019). Mediator complex condensation was shown to drive transcriptional control (Boija et al., 2018) and interestingly, FIT was also shown to interact with Mediator complexes, directly and indirectly (Yang et al., 2014; Zhang et al., 2014). Besides, other studies suggest TF condensation to be involved in transcriptional regulation (Kaiserli et al., 2015; Huang et al., 2022). Possibly, the basic region of FIT and bHLH039 might be accessible for DNA binding either within or outside of NBs to regulate target genes (Boija et al., 2018; Brodsky et al., 2020). In further studies, it will be interesting to analyze whether DNA and mRNA FIT targets are present inside FIT NBs and whether FIT may also interact directly with other speckle components.

As we focused to characterize the phenomenon, the physiological integration and regulation of the induction of FIT NB formation can be subject of future studies. The rapid speed by which FIT NB appeared within 5 min in *N. benthamiana* leaf cells speaks in favor of protein rearrangement rather than protein synthesis. The long duration of FIT NB formation after blue light induction in Arabidopsis roots suggests that signal transduction was more complex and possibly involved intracellular or even cell-to-cell and long-distance leaf-to-root signaling. In how far a long-distance signal or a signaling cascade triggered by light is involved in FIT NB formation in roots remains to be investigated, but CRY1/CRY2 and HY5 are promising candidates for further studies (Gao et al., 2021; Guo et al., 2021). In order to undergo phase separation, a certain protein concentration must be reached (Bracha et al., 2018). Since FIT protein is subject of proteasomal turnover in roots, FIT NB formation may depend on FIT protein interaction partners in roots that need to be activated (Lingam et al., 2011; Meiser et al., 2011).

In summary, FIT engages in protein complexes inside dynamic NBs. FIT NBs contain active TF complexes for iron acquisition gene expression (**Figure 8A**). FIT NBs are speckles that link transcriptional with post-transcriptional regulation (**Figure 8B**). The appearance of FIT NBs is inducible by light, and light-regulated PB components are connected with FIT NBs and vice versa. It will be interesting in the future to test hormonal and environmental triggers that may stabilize FIT protein prior to examining the initiation of FIT NBs in root physiological situations and to investigate the effects on transcriptional and posttranscriptional regulation of FIT targets.

Materials and methods

Plant material and growth conditions

Arabidopsis thaliana 2x35S$_{pro}$:FIT-GFP/*fit-3* seedlings (Gratz et al., 2019) were used for localization studies. Seeds were sterilized and grown upright on Hoagland medium plates (macronutrients: 1.5 mM $Ca(NO_3)_2 \cdot 4H_2O$, 0.5 mM KH_2PO_4, 1.25 mM KNO_3, 0.75 mM $MgSO_4 \cdot 7H_2O$; micronutrients: 0.075 µM $(NH_4)6Mo_7O_{24} \cdot 4H_2O$, 1.5 µM $CuSO_4 \cdot 5H_2O$, 50 µM H_3BO_3, 50 µM KCl, 10 µM $MnSO_4 \cdot H_2O$, 2 µM $ZnSO_4 \cdot 7H_2O$; 1.4 % (w/v) plant agar, 1 % (w/v) sucrose, pH 5.8) with no iron supply for 5 d under long day conditions (16 h light/8 h dark) at 21°C in a plant chamber (CLF Plant Climatics) under white light (120 µmol m^{-2} s^{-1}). *Nicotiana benthamiana* plants for transient protein expression were grown in the greenhouse facility for approx. 4 weeks under long day conditions (16 h light/8 h dark).

Microscopy of *Arabidopsis thaliana* seedlings

Protein localization studies in roots of 5-d-old seedlings of the *Arabidopsis thaliana* line 2x35S$_{pro}$:FIT-GFP/*fit-3* (Gratz et al., 2019) were performed with the widefield microscope ELYRA PS (Zeiss) equipped with a EMCCD camera. Whole seedlings were exposed to 488 nm laser light for several minutes. GFP was excited with a 488 nm laser and detected with a BP 495-575 + LP 750 beam splitter. Images were acquired with the C-Apochromat 63x/1.2 W Korr M27 (Zeiss) objective, pixel dwell time of 1.6 µs and frame size of 512x512. Pictures were processed with the manufacturer's software ZEN lite (Zeiss).

Generation of fluorescent constructs

All constructs used in this study are listed in **Supplemental Table S1**. Generation of fluorescent translational C-terminal fusion of PIF3 and PIF4 with mCherry was performed with Gateway Cloning. CDS of *PIF3* was amplified with the PIF3 GW fw (5`-GGGGACAAGTTTGTACAAAAAAGCAGGCTATGCCTCTGTTTGAGCTT-3') and PIF3 GW rv (5'-GGGGACCACTTTGTACAAGAAAGCTGGGTCCGACGATCCACAAAACTG-3') primers, and CDS of *PIF4* was amplified with the PIF4 GW fw (5'-GGGGACAAGTTTGTACAAAAAAGCAGGCTATGGAACACCAAGGTTGG-3') and PIF4 GW rv (5'-GGGGACCACTTTGTACAAGAAAGCTGGGTCGTGGTCCAAACGAGAACC-3') primers, and introduced into the entry vector pDONR207 via the BP reaction (Life Technologies) and subsequently into the inducible pABind 35S$_{pro}$:mCherry destination

vector (Bleckmann et al., 2010) via the LR reaction (Life Technologies). Finally, *Rhizobium radiobacter* was transformed with the constructs for transient transformation of *Nicotiana benthamiana* leaf epidermal cells.

Transient transformation of *Nicotiana benthamiana* leaf epidermal cells

Transient protein expression was performed in *Nicotiana benthamiana* leaf epidermal cells according to Bleckmann et al. (2010). This was performed for localization studies, FRAP measurements, anisotropy (homo-FRET) measurements, FRET-FLIM measurements, and NB quantification. Cultures of *Rhizobium radiobacter* containing the construct of interest (**Supplemental Table S1**) were incubated overnight and cell were pelleted and dissolved in AS medium (250 µM acetosyringone (in DMSO), 5 % (w/v) sucrose, 0.01 % (v/v) silwet, 0.01 % (w/v) glucose). An OD_{600nm} of 0.4 was set for all constructs. A *Rhizobium radiobacter* strain containing the silencing repressor p19 vector (Shamloul et al., 2014) was used additionally for bHLH039-mCherry to enhance expression. After 1 h incubation on ice the suspension was infiltrated with a syringe into the abaxial side of the leaf. *Nicotiana benthamiana* plants were kept under long day conditions (16 h light/8 h dark) in the laboratory after infiltration. Imaging was performed 2-3 d after infiltration. Expression of constructs with an inducible 35S promoter was induced 16 h prior to imaging with β-estradiol (20 µM β-estradiol (in DMSO), 0.1 % (v/v) Tween 20).

Confocal microscopy

For localization studies a confocal laser scanning microscope LSM780 (Zeiss) was used. Imaging was controlled by the ZEN 2.3 SP1 FP3 (Black) (Zeiss) software. GFP was excited with a 488 nm laser and detected in the range of 491-553 nm. mCherry and mRFP were excited with a 561 nm laser and detected in the range of 562-626 nm. Fluorophore crosstalk was minimized by splitting of the excitation tracks and reduction of emission spectrum overlap. Images were acquired with the C-Apochromat 40x/1.20 W Korr M27 (Zeiss) objective, zoom factor of 8, pinhole set to 1,00 AU, pixel dwell time of 1.27 µs and frame size of 1.024x1.024. Z-stacks for quantification were taken with the same settings, except with pixel dwell time of 0.79 µs and frame size of 512x512. Pictures were processed with the manufacturer's software ZEN lite (Zeiss).

Standardized FIT NB analysis procedure

Following *Nicotiana benthamiana* leaf infiltration with *Rhizobium radiobacter*, FIT-GFP protein expression was induced after 2-3 d by β-estradiol, as described above. 16 h later, a leaf disc was excised and FIT-GFP fluorescence signals were recorded (t=0). The leaf disc was excited with 488 nm laser light for 1 min. 5 min later, FIT-GFP accumulation in FIT NBs was observed (t= 5 min). See **Supplemental Figure S1**. This procedure was modified by using different time points for NB analysis and different constructs (**Supplemental Table S1**) and co-expression as indicated in the text. Imaging was performed at the respective wavelengths for detection of GFP and mRFP/mCherry.

FRAP measurements

FRAP measurements (Bancaud et al., 2010; Trofimov et al., 2019) were performed at the confocal laser scanning microscope LSM780 (Zeiss). Imaging was controlled by the ZEN 2.3 SP1 FP3 (Black) (Zeiss) software. GFP was excited with a 488 nm laser and detected in the range of 491-553 nm. Images were acquired with the C-Apochromat 40x/1.20 W Korr M27 (Zeiss) objective, zoom factor of 8, pinhole set to 2,43 AU, pixel dwell time of 1.0 µs, frame size of 256x256, and 300 frames. After 20 frames, a NB was bleached with 50 iterations and 100% 488 nm laser power. Fluorescence intensity was recorded for the bleached NB (ROI), a non-bleached region equal in size to the NB (BG) as well as for the total image (Tot). Values were calculated and processed in Excel (Microsoft Corporation). Background subtraction and normalization to calculate the relative fluorescence intensity was performed as follows: [(ROI(t)-BG(t)/Tot(T)-BG(t))*(Tot(t0)-BG(t0)/ROI(t0)-BG(t0))]. The mobile fraction was calculated as follows: $[(F_{end}-F_{post})/(F_{pre}-F_{post})*100]$. F_{pre} marks the average of the 20 values before bleaching, F_{post} marks the value right after the bleaching, and F_{end} marks the average of the 280 values after the bleaching. Pictures were processed with the manufacturer's software ZEN lite (Zeiss).

Anisotropy (homo-FRET) measurements

Anisotropy measurements (Stahl et al., 2013; Weidtkamp-Peters et al., 2022) were performed at the confocal laser scanning microscope LSM780 (Zeiss) equipped with a polarization beam splitter, bandpass filter (520/35), and a single-photon counting device HydraHarp (PicoQuant) with avalanche photo diodes (τ-SPADs). Emission was detected in parallel and perpendicular orientation. Rhodamine 110 was used to determine the G

643 factor to correct for the differential parallel and perpendicular detector sensitivity.
644 Calibration of the system was performed for every experiment and measurements were
645 conducted in darkness. Free GFP and GFP-GFP were used as references for mono- and
646 dimerization, respectively. GFP was excited with a linearly polarized pulsed (32 MHz)
647 485 nm laser and 0.05-1 µW output power. Measurements were recorded with a C-
648 Apochromat 40x/1.20 W Korr M27 (Zeiss) objective, zoom factor of 8, pixel dwell time of
649 12.5 µs, objective frame size of 256x256, and 40 frames. Measurements were controlled
650 with the manufacturer's ZEN 2.3 SP1 FP3 (Black) (Zeiss) software and SymPhoTime 64
651 (PicoQuant) software. SymPhoTime 64 (PicoQuant) software was used for analysis in the
652 respective regions of interest (whole nucleus, NB, NP) and to generate color-coded FA
653 value images. Minimal photon count was set to 200.

654 **FRET-FLIM measurements**

655 FRET-FLIM measurements (Borst and Visser, 2010; Weidtkamp-Peters and Stahl,
656 2017) were taken at the confocal laser scanning microscope FV3000 (Olympus) equipped
657 with a multi-photon counting device MultiHarp 150 (PicoQuant) with avalanche photo
658 diodes (τ-SPADs) and bandpass filter (520/35). Erythrosine B (quenched in saturated
659 potassium iodide) was used to record the Instrument Response Function to correct for the
660 time between laser pulse and detection. Calibration of the system was performed for every
661 experiment and measurements were conducted in darkness. FIT-GFP and
662 FITmSS271AA-GFP were used as negative controls (donor only), FIT-GFP or
663 FITmSS271AA-GFP (donor) and bHLH039-mCherry (acceptor) as FRET pair. GFP was
664 excited with a linearly polarized pulsed (32 MHz) 485 nm laser and 0.01-0.1 µW output
665 power. Measurements were recorded with a UPLSAPO 60XW (Olympus) objective, zoom
666 factor of 8, pixel dwell time of 12.5 µs, objective frame size of 256x256, and 60 frames.
667 Measurements were controlled with the manufacturer's FV31S-SW (Olympus) software
668 and SymPhoTime 64 (PicoQuant) software. SymPhoTime 64 (PicoQuant) software was
669 used for analysis in the respective regions of interest (whole nucleus, NB, NP) and to
670 generate color-coded fluorescence lifetime value images. Number of parameters for the
671 fit depended on the region of interest.

672 **Circularity quantification**

673 Circularity quantification was performed with the software ImageJ (National
674 Institutes of Health). Full intensity projection images were generated from Z-stacks in the

ZEN lite (Zeiss) software and exported as TIFF (no compression, all dimensions). Images were duplicated in ImageJ and converted to RGB and 8-bit. Correct scale was set (in µm) under 'Analyze' - 'Set Scale'. Threshold for the intensity limit (areas below that limit were not considered for quantification) was set under 'Image' - 'Adjust' - 'Threshold' and was set manually for every image. To separate the nuclear bodies better, 'Process' - 'Binary' - 'Watershed' was used. Parameters that should be quantified were selected under 'Analyze' - 'Set Measurements'. To perform the analysis, 'Analyze' - 'Analyze Particles' was selected. Calculated values were further processed in Excel (Microsoft Corporation).

Nuclear body quantification

Nuclear body quantification was performed with the software ImageJ (National Institutes of Health) and additional plugin '3D Object Counter'. Z-stacks were exported from the ZEN lite (Zeiss) software as TIFF (no compression, all dimensions) first. In ImageJ, Z-stacks were converted to RGB and 8-bit. Correct scale was set (in µm) under 'Properties'. Parameters that should be quantified were selected under 'Plugins' - '3D Object Counter' - 'Set 3D Measurements'. To perform the analysis, 'Plugins' - '3D Object Counter' - '3D object counter' was selected. Threshold for the intensity limit (areas below that limit were not considered for quantification) was set manually for every z-stack. Calculated values were further processed in Excel (Microsoft Corporation). Only size between 0,01-15 µm³ was considered.

Protein domain prediction

IDRs in FIT/FITmSS271AA were predicted with the tool PONDR-VLXT (www.pondr.com, Molecular Kinetics, Inc.). According to the sequence of the protein, a PONDR score was determined for each amino acid. A score above 0.5 indicates intrinsic disorder. The bHLH domain of FIT was predicted with InterPro (www.ebi.ac.uk/interpro, EMBL-EBI).

Statistical analysis

Line and bar diagrams represent the mean and standard deviation. Box plots show 25-75 percentile with min-max whiskers, mean as small square and median as line. Graphs and statistical analysis were created and performed with OriginPro (OriginLab Corporation). Data was tested for normal distribution with the Shapiro-Wilk test. Statistical significance of data with normal distribution was tested by one-way Anova with Tukey

post-hoc test. Statistical significance of data with non-normal distribution was tested by Mann-Whitney test. Different letters indicate statistically significant differences ($P < 0.05$). Illustrations were created with BioRender.com.

Accession numbers

Sequence data from this article can be found in the EMBL/GenBank data libraries under accession numbers*:* *bHLH039* (AT3G56980), *COILIN* (AT1G13030), *FIT* (AT2G28160), *P15H1* (AT1G11570), *PIF3* (AT1G09530), *PIF4* (AT2G43010), *PININ* (AT1G15200), *SR45* (AT1G16610), *SRm102* (AT2G29210), *U2B"* (AT2G30260), *UAP56H2* (AT5G11170), and *ZAT12* (AT5G59820).

Figures

Figure 1. FIT accumulated in nuclear condensates, termed FIT nuclear bodies (NBs) in a light-inducible manner, most likely following liquid-liquid phase separation (LLPS).

Figure 2. The FIT C-terminal Ser271/272 site was important for the capacity of FIT to localize to NBs.

Figure 3. FIT was present in homodimeric protein complexes in NBs, dependent on Ser271/272 site.

Figure 4. FIT was present in heterodimeric protein complexes with bHLH039 in NBs, dependent on Ser271/272 site.

Figure 5. Two NB markers and splicing components were present in NBs in which FIT accumulated after the light trigger, whereas they were not part of FIT NBs (designated type II).

Figure 6. Three NB markers and speckle components became localized in FIT NBs and colocalized fully with FIT (designated type III), suggesting that FIT NBs have speckle function.

Figure 7. FIT colocalized with photobody (PB) markers in distinct PBs.

Figure 8. Schematic summary models illustrating the dynamics of FIT NB formation, suggesting that FIT NBs are related to transcriptional and posttranscriptional regulation in speckles.

Supplemental Data

Supplemental Figure S1. A standardized FIT NB analysis procedure was developed to analyze the characteristics and dynamics of FIT NBs. (Supports Figure 1)

Supplemental Figure S2. An intrinsically disordered region, $IDR^{Ser271/272}$, is present in the FIT C-terminus and disrupted in the FITmSS271AA mutant. (Supports Figure 2, 3, and 4)

Supplemental Figure S3. FIT NBs did not colocalize with Cajal body components (designated type I). (Supports Figure 5 and 6)

Supplemental Figure S4. Type II and III NB markers are similarly localized upon single expression as upon co-expression with FIT, except PININ. (Supports Figure 5 and 6)

Supplemental Figure S5. PB markers are similarly localized upon single expression and upon co-expression with FIT. (Supports Figure 7)

Supplemental Table S1. List of vectors used in this study.

Supplemental Movie S1. Light induction triggers the formation of NBs with FIT and FITmSS271AA with different dynamics. (Supports Figure 1 and 2)

Acknowledgements

We thank Elke Wieneke and Monique Eutebach (Institute of Botany, Heinrich-Heine-University, Düsseldorf, Germany) for excellent technical assistance. We thank Rebecca C. Burkart (Institute of Developmental Genetics, Heinrich-Heine-University, Düsseldorf, Germany), Sebastian Hänsch and Stefanie Weidtkamp-Peters (Center for Advanced Imaging, Heinrich-Heine-University, Düsseldorf, Germany) for help and advice with microscopy and data analysis. K.T. is an associate member of the DFG-funded International Graduate School for Plant Science iGRAD*plant* (IRTG 2466 "Network, exchange, and training program to understand plant resource allocation"), Düsseldorf, Germany.

Funding

This work was funded by Deutsche Forschungsgemeinschaft (DFG, German Research Foundation) under GRK F020512056 (NEXT*plant*), SFB 1208 project B05, and Germany´s Excellence Strategy – EXC-2048/1 – project ID 390686111. Funding for instrumentation: Zeiss ELYRA PS: DFG- INST 208/613-1 FUGG; Zeiss LSM780 + 4-channel FLIM extension (Picoquant): DFG- INST 208/551-1 FUGG; Olympus FV3000 Confocal Laser Scanning Microscope with 4-channel FLIM extension (PicoQuant rapidFLIM): DFG- INST 1358/44-1 FUGB.

K.T., R.I., Y.S., P.B. and T.B. designed the research; K.T. performed research; K.T., R.I., Y.S., and T.B. analyzed data; R.G. contributed key materials; K.T. wrote the paper; P.B. acquired funding; all authors reviewed and edited the article.

References

Ali, G.S., Golovkin, M., and Reddy, A.S.N. (2003). Nuclear localization and in vivo dynamics of a plant-specific serine/arginine-rich protein. Plant J. **36**: 883–893.

Bancaud, A., Huet, S., Rabut, G., and Ellenberg, J. (2010). Fluorescence Perturbation Techniques to Study Mobility and Molecular Dynamics of Proteins in Live Cells: FRAP, Photoactivation, Photoconversion, and FLIP. Cold Spring Harb. Protoc.: 1303–1325.

Bauer, D., Viczían, A., Kircher, S., Nobis, T., Nitschke, R., Kunkel, T., Panigrahi, K.C.S., Ádám, É., Fejes, E., Schäfer, E., and Nagy, F. (2004). Constitutive Photomorphogenesis 1 and Multiple Photoreceptors Control Degradation of Phytochrome Interacting Factor 3, a Transcription Factor Required for Light Signaling in Arabidopsis. Plant Cell **16**: 1433–1445.

Bauer, P., Ling, H.Q., and Guerinot, M. Lou (2007). FIT, the FER-LIKE IRON DEFICIENCY INDUCED TRANSCRIPTION FACTOR in Arabidopsis. Plant Physiol. Biochem. **45**: 260–261.

Bi, Y. et al. (2021). Arabidopsis ACINUS is O-glycosylated and regulates transcription and alternative splicing of regulators of reproductive transitions. Nat. Commun. **12**: 1–13.

Bleckmann, A., Weidtkamp-Peters, S., Seidel, C.A.M., and Simon, R. (2010). Stem Cell Signaling in Arabidopsis Requires CRN to Localize CLV2 to the Plasma Membrane. Plant Physiol. **152**: 166–176.

Boija, A. et al. (2018). Transcription Factors Activate Genes through the Phase-Separation Capacity of Their Activation Domains. Cell **175**: 1842–1855.

Borst, J.W. and Visser, A.J.W.G. (2010). Fluorescence lifetime imaging microscopy in life sciences. Meas. Sci. Technol. **21**: 1–21.

Bracha, D., Walls, M.T., Wei, M.T., Zhu, L., Kurian, M., Avalos, J.L., Toettcher, J.E., and Brangwynne, C.P. (2018). Mapping Local and Global Liquid Phase Behavior in Living Cells Using Photo-Oligomerizable Seeds. Cell **175**: 1467–1480.

Brumbarova, T. and Ivanov, R. (2019). The Nutrient Response Transcriptional Regulome of Arabidopsis. iScience **19**: 358–368.

Burkart, R.C., Strotmann, V.I., Kirschner, G.K., Akinci, A., Czempik, L., Dolata, A., Maizel, A., Weidtkamp-Peters, S., and Stahl, Y. (2022). PLETHORA-WOX5 interaction and subnuclear localization control Arabidopsis root stem cell

maintenance. EMBO Rep. **23**: 1–18.

Van Buskirk, E.K., Reddy, A.K., Nagatani, A., and Chen, M. (2014). Photobody Localization of Phytochrome B Is Tightly Correlated with Prolonged and Light-Dependent Inhibition of Hypocotyl Elongation in the Dark. Plant Physiol. **165**: 595–607.

Colangelo, E.P. and Guerinot, M. Lou (2004). The Essential Basic Helix-Loop-Helix Protein FIT1 Is Required for the Iron Deficiency Response. Plant Cell **16**: 3400–3412.

Collier, S., Pendle, A., Boudonck, K., van Rij, T., Dolan, L., and Shaw, P. (2006). A Distant Coilin Homologue Is Required for the Formation of Cajal Bodies in Arabidopsis. Mol. Biol. Cell **17**: 2942–2951.

Cui, Y., Chen, C.L., Cui, M., Zhou, W.J., Wu, H.L., and Ling, H.Q. (2018). Four IVa bHLH Transcription Factors Are Novel Interactors of FIT and Mediate JA Inhibition of Iron Uptake in Arabidopsis. Mol. Plant **11**: 1166–1183.

Emenecker, R.J., Holehouse, A.S., and Strader, L.C. (2020). Emerging Roles for Phase Separation in Plants. Dev. Cell **55**: 69–83.

Emenecker, R.J., Holehouse, A.S., and Strader, L.C. (2021). Sequence determinants of in cell condensate morphology, dynamics, and oligomerization as measured by number and brightness analysis. Cell Commun. Signal. **19**: 1–15.

Fanara, S., Schloesser, M., Hanikenne, M., and Motte, P. (2022). Altered metal distribution in the sr45-1 Arabidopsis mutant causes developmental defects. Plant J. **110**: 1332–1352.

Fang, X., Wang, L., Ishikawa, R., Li, Y., Fiedler, M., Liu, F., Calder, G., Rowan, B., Weigel, D., Li, P., and Dean, C. (2019). Arabidopsis FLL2 promotes liquid–liquid phase separation of polyadenylation complexes. Nature **569**: 265–269.

Galganski, L., Urbanek, M.O., and Krzyzosiak, W.J. (2017). Nuclear speckles: Molecular organization, biological function and role in disease. Nucleic Acids Res. **45**: 10350–10368.

Gao, F., Robe, K., Bettembourg, M., Navarro, N., Rofidal, V., Santoni, V., Gaymard, F., Vignols, F., Roschzttardtz, H., Izquierdo, E., and Dubos, C. (2020). The Transcription Factor bHLH121 Interacts with bHLH105 (ILR3) and Its Closest Homologs to Regulate Iron Homeostasis in Arabidopsis. Plant Cell **32**: 508–524.

Gao, Y.Q., Bu, L.H., Han, M.L., Wang, Y.L., Li, Z.Y., Liu, H.T., and Chao, D.Y. (2021).

Long-distance blue light signalling regulates phosphate deficiency-induced primary root growth inhibition. Mol. Plant **14**: 1539–1553.

Gratz, R. et al. (2019). CIPK11-Dependent Phosphorylation Modulates FIT Activity to Promote Arabidopsis Iron Acquisition in Response to Calcium Signaling. Dev. Cell **48**: 726–740.

Gratz, R., Brumbarova, T., Ivanov, R., Trofimov, K., Tünnermann, L., Ochoa-Fernandez, R., Blomeier, T., Meiser, J., Weidtkamp-Peters, S., Zurbriggen, M., and Bauer, P. (2020). Phospho-mutant activity assays provide evidence for alternative phospho-regulation pathways of the transcription factor FER-LIKE IRON DEFICIENCY-INDUCED TRANSCRIPTION FACTOR. New Phytol. **225**: 250–267.

Guo, Z., Xu, J., Wang, Y., Hu, C., Shi, K., Zhou, J., Xia, X., Zhou, Y., Foyer, C.H., and Yu, J. (2021). The phyB-dependent induction of HY5 promotes iron uptake by systemically activating FER expression. EMBO Rep. **22**: 1–15.

Huang, X., Xiao, N., Zou, Y., Xie, Y., Tang, L., Zhang, Y., Yu, Y., Li, Y., and Xu, C. (2022). Heterotypic transcriptional condensates formed by prion-like paralogous proteins canalize flowering transition in tomato. Genome Biol. **23**: 1–21.

Jakoby, M., Wang, H.Y., Reidt, W., Weisshaar, B., and Bauer, P. (2004). FRU (BHLH029) is required for induction of iron mobilization genes in Arabidopsis thaliana. FEBS Lett. **577**: 528–534.

Jung, J.-H. et al. (2020). A prion-like domain in ELF3 functions as a thermosensor in Arabidopsis. Nature **585**: 256–260.

Kaiserli, E., Páldi, K., O'Donnell, L., Batalov, O., Pedmale, U. V., Nusinow, D.A., Kay, S.A., and Chory, J. (2015). Integration of Light and Photoperiodic Signaling in Transcriptional Nuclear Foci. Dev. Cell **35**: 311–321.

Kalinina, N.O., Makarova, S., Makhotenko, A., Love, A.J., and Taliansky, M. (2018). The Multiple Functions of the Nucleolus in Plant Development, Disease and Stress Responses. Front. Plant Sci. **9**: 1–19.

Kammel, C., Thomaier, M., Sørensen, B.B., Schubert, T., Längst, G., Grasser, M., and Grasser, K.D. (2013). Arabidopsis DEAD-Box RNA Helicase UAP56 Interacts with Both RNA and DNA as well as with mRNA Export Factors. PLoS One **8**: 1–12.

Kanwar, P., Baby, D., and Bauer, P. (2021). Interconnection of iron and osmotic stress signalling in plants: is FIT a regulatory hub to cross-connect abscisic acid responses? Plant Biol. **23**: 31–38.

Kim, D.W., Jeon, S.J., Hwang, S.M., Hong, J.C., and Bahk, J.D. (2016). The C3H-type zinc finger protein GDS1/C3H42 is a nuclear-speckle-localized protein that is essential for normal growth and development in Arabidopsis. Plant Sci. **250**: 141–153.

Kim, S.A., Lacroix, I.S., Gerber, S.A., and Guerinot, M. Lou (2019). The iron deficiency response in Arabidopsis thaliana requires the phosphorylated transcription factor URI. Proc. Natl. Acad. Sci. **116**: 24933–24942.

Kircher, S., Gil, P., Kozma-Bognár, L., Fejes, E., Speth, V., Husselstein-Muller, T., Bauer, D., Ádám, É., Schäfer, E., and Nagy, F. (2002). Nucleocytoplasmic Partitioning of the Plant Photoreceptors Phytochrome A, B, C, D, and E Is Regulated Differentially by Light and Exhibits a Diurnal Rhythm. Plant Cell **14**: 1541–1555.

Lafontaine, D.L.J., Riback, J.A., Bascetin, R., and Brangwynne, C.P. (2021). The nucleolus as a multiphase liquid condensate. Nat. Rev. Mol. Cell Biol. **22**: 165–182.

Le, C.T.T., Brumbarova, T., Ivanov, R., Stoof, C., Weber, E., Mohrbacher, J., Fink-Straube, C., and Bauer, P. (2016). ZINC FINGER OF ARABIDOPSIS THALIANA12 (ZAT12) Interacts with FER-LIKE IRON DEFICIENCY-INDUCED TRANSCRIPTION FACTOR (FIT) Linking Iron Deficiency and Oxidative Stress Responses. Plant Physiol. **170**: 540–557.

Leivar, P. and Monte, E. (2014). PIFs: Systems Integrators in Plant Development. Plant Cell **26**: 56–78.

Leonelli, L., Erickson, E., Lyska, D., and Niyogi, K.K. (2016). Transient expression in Nicotiana benthamiana for rapid functional analysis of genes involved in non-photochemical quenching and carotenoid biosynthesis. Plant J. **88**: 375–386.

Li, W., Lin, W.-D., Ray, P., Lan, P., and Schmidt, W. (2013). Genome-Wide Detection of Condition-Sensitive Alternative Splicing in Arabidopsis Roots. Plant Physiol. **162**: 1750–1763.

Li, X., Zhang, H., Ai, Q., Liang, G., and Yu, D. (2016). Two bHLH Transcription Factors, bHLH34 and bHLH104, Regulate Iron Homeostasis in Arabidopsis thaliana. Plant Physiol. **170**: 2478–2493.

Liang, G., Zhang, H., Li, X., Ai, Q., and Yu, D. (2017). bHLH transcription factor bHLH115 regulates iron homeostasis in Arabidopsis thaliana. J. Exp. Bot. **68**: 1743–1755.

Lin, C.L., Leu, S., Lu, M.C., and Ouyang, P. (2004). Over-expression of SR-cyclophilin, an interaction partner of nuclear pinin, releases SR family splicing factors from nuclear speckles. Biochem. Biophys. Res. Commun. **321**: 638–647.

Lingam, S., Mohrbacher, J., Brumbarova, T., Potuschak, T., Fink-Straube, C., Blondet, E., Genschik, P., and Bauer, P. (2011). Interaction between the bHLH Transcription Factor FIT and ETHYLENE INSENSITIVE3/ETHYLENE INSENSITIVE3-LIKE1 Reveals Molecular Linkage between the Regulation of Iron Acquisition and Ethylene Signaling in Arabidopsis. Plant Cell **23**: 1815–1829.

Lorković, Z.J., Hilscher, J., and Barta, A. (2008). Co-localisation studies of Arabidopsis SR splicing factors reveal different types of speckles in plant cell nuclei. Exp. Cell Res. **314**: 3175–3186.

Lorković, Z.J., Hilscher, J., and Barta, A. (2004). Use of Fluorescent Protein Tags to Study Nuclear Organization of the Spliceosomal Machinery in Transiently Transformed Living Plant Cells. Mol. Biol. Cell **15**: 3233–3243.

Love, A.J., Yu, C., Petukhova, N. V., Kalinina, N.O., Chen, J., and Taliansky, M.E. (2017). Cajal bodies and their role in plant stress and disease responses. RNA Biol. **14**: 779–790.

Martin, K., Kopperud, K., Chakrabarty, R., Banerjee, R., Brooks, R., and Goodin, M.M. (2009). Transient expression in Nicotiana benthamiana fluorescent marker lines provides enhanced definition of protein localization, movement and interactions in planta. Plant J. **59**: 150–162.

Meiser, J., Lingam, S., and Bauer, P. (2011). Posttranslational Regulation of the Iron Deficiency Basic Helix-Loop-Helix Transcription Factor FIT Is Affected by Iron and Nitric Oxide. Plant Physiol. **157**: 2154–2166.

Meyer, H.M. (2020). In search of function : nuclear bodies and their possible roles as plant environmental sensors. Curr. Opin. Plant Biol. **58**: 33–40.

Mikulski, P., Wolff, P., Lu, T., Nielsen, M., Echevarria, E.F., Zhu, D., Questa, J.I., Saalbach, G., Martins, C., and Dean, C. (2022). VAL1 acts as an assembly platform co-ordinating co-transcriptional repression and chromatin regulation at Arabidopsis FLC. Nat. Commun. **13**: 1–12.

Naranjo-Arcos, M.A., Maurer, F., Meiser, J., Pateyron, S., Fink-Straube, C., and Bauer, P. (2017). Dissection of iron signaling and iron accumulation by overexpression of subgroup Ib bHLH039 protein. Sci. Rep. **7**: 1–12.

Owen, I. and Shewmaker, F. (2019). The Role of Post-Translational Modifications in the Phase Transitions of Intrinsically Disordered Proteins. Int. J. Mol. Sci. **20**: 1–14.

Pardi, S.A. and Nusinow, D.A. (2021). Out of the Dark and Into the Light: A New View of Phytochrome Photobodies. Front. Plant Sci. **12**: 1–15.

Pendle, A.F., Cark, G.P., Boon, R., Lewandowska, D., Lam, Y.W., Andersen, J., Mann, M., Lamond, A.I., Brown, J.W.S., and Shaw, P.J. (2005). Proteomic Analysis of the Arabidopsis Nucleolus Suggests Novel Nucleolar Functions. Mol. Biol. Cell **16**: 260–269.

Pham, V.N., Kathare, P.K., and Huq, E. (2018). Phytochromes and Phytochrome Interacting Factors. Plant Physiol. **176**: 1025–1038.

Powers, S.K. et al. (2019). Nucleo-cytoplasmic Partitioning of ARF Proteins Controls Auxin Responses in Arabidopsis thaliana. Mol. Cell **76**: 177–190.

Qiu, Y., Li, M., Kim, R.J.A., Moore, C.M., and Chen, M. (2019). Daytime temperature is sensed by phytochrome B in Arabidopsis through a transcriptional activator HEMERA. Nat. Commun. **10**: 1–13.

Qiu, Y., Pasoreck, E.K., Yoo, C.Y., He, J., Wang, H., Bajracharya, A., Li, M., Larsen, H.D., Cheung, S., and Chen, M. (2021). RCB initiates Arabidopsis thermomorphogenesis by stabilizing the thermoregulator PIF4 in the daytime. Nat. Commun. **12**: 1–13.

Reddy, A.S.N., Day, I.S., Gohring, J., and Barta, A. (2012). Localization and Dynamics of Nuclear Speckles in Plants. Plant Physiol. **158**: 67–77.

Riback, J.A., Zhu, L., Ferrolino, M.C., Tolbert, M., Mitrea, D.M., Sanders, D.W., Wei, M.-T., Kriwacki, R.W., and Brangwynne, C.P. (2020). Composition-dependent thermodynamics of intracellular phase separation. Nature **581**: 209–214.

Römheld, V. and Marschner, H. (1986). Mobilization of iron in the rhizosphere of different plant species. Adv. Plant Nutr. **2**: 155–204.

Salladini, E., Jørgensen, M.L.M., Theisen, F.F., and Skriver, K. (2020). Intrinsic Disorder in Plant Transcription Factor Systems: Functional Implications. Int. J. Mol. Sci. **21**: 1–35.

Schwarz, B. and Bauer, P. (2020). FIT, a regulatory hub for iron deficiency and stress signaling in roots, and FIT-dependent and -independent gene signatures. J. Exp. Bot. **71**: 1694–1705.

Shamloul, M., Trusa, J., Mett, V., and Yusibov, V. (2014). Optimization and Utilization

of Agrobacterium-mediated Transient Protein Production in Nicotiana. J. Vis. Exp.: 1–13.

Shin, Y., Berry, J., Pannucci, N., Haataja, M.P., Toettcher, J.E., and Brangwynne, C.P. (2017). Spatiotemporal Control of Intracellular Phase Transitions Using Light-Activated optoDroplets. Cell **168**: 159–171.

Stahl, Y. et al. (2013). Moderation of Arabidopsis root Stemness by CLAVATA1 and ARABIDOPSIS CRINKLY4 Receptor Kinase Complexes. Curr. Biol. **23**: 362–371.

Strader, L., Weijers, D., and Wagner, D. (2022). Plant transcription factors — being in the right place with the right company. Curr. Opin. Plant Biol. **65**: 102136.

Tarczewska, A. and Greb-Markiewicz, B. (2019). The Significance of the Intrinsically Disordered Regions for the Functions of the bHLH Transcription Factors. Int. J. Mol. Sci. **20**: 1–20.

Trinkle-Mulcahy, L. and Sleeman, J.E. (2017). The Cajal body and the nucleolus: "In a relationship" or "It's complicated"? RNA Biol. **14**: 739–751.

Trofimov, K., Ivanov, R., Eutebach, M., Acaroglu, B., Mohr, I., Bauer, P., and Brumbarova, T. (2019). Mobility and localization of the iron deficiency-induced transcription factor bHLH039 change in the presence of FIT. Plant Direct **3**: 1–11.

Wang, H.Y., Klatte, M., Jakoby, M., Bäumlein, H., Weisshaar, B., and Bauer, P. (2007). Iron deficiency-mediated stress regulation of four subgroup Ib BHLH genes in Arabidopsis thaliana. Planta **226**: 897–908.

Wang, N., Cui, Y., Liu, Y., Fan, H., Du, J., Huang, Z., Yuan, Y., Wu, H., and Ling, H.Q. (2013). Requirement and Functional Redundancy of Ib Subgroup bHLH Proteins for Iron Deficiency Responses and Uptake in Arabidopsis thaliana. Mol. Plant **6**: 503–513.

Wang, X., Jiang, B., Gu, L., Chen, Y., Mora, M., Zhu, M., Noory, E., Wang, Q., and Lin, C. (2021). A photoregulatory mechanism of the circadian clock in Arabidopsis. Nat. Plants **7**: 1397–1408.

Wedepohl, K.H. (1995). The composition of the continental crust. Geochim. Cosmochim. Acta **59**: 1217–1232.

Weidtkamp-Peters, S., Rehwald, S., and Stahl, Y. (2022). Homo-FRET Imaging to Study Protein–Protein Interaction and Complex Formation in Plants. In Plant Synthetic Biology: Methods and Protocols, M.D. Zurbriggen, ed (Springer US: New York, NY), pp. 197–208.

1000 **Weidtkamp-Peters, S. and Stahl, Y.** (2017). The Use of FRET/FLIM to Study Proteins
1001 Interacting with Plant Receptor Kinases. In Plant Receptor Kinases: Methods and
1002 Protocols, R.B. Aalen, ed (Springer New York: New York, NY), pp. 163–175.
1003 **Wild, M., Davière, J.M., Regnault, T., Sakvarelidze-Achard, L., Carrera, E., Lopez**
1004 **Diaz, I., Cayrel, A., Dubeaux, G., Vert, G., and Achard, P.** (2016). Tissue-Specific
1005 Regulation of Gibberellin Signaling Fine-Tunes Arabidopsis Iron-Deficiency
1006 Responses. Dev. Cell **37**: 190–200.
1007 **Yang, Y., Ou, B., Zhang, J., Si, W., Gu, H., Qin, G., and Qu, L.-J.** (2014). The
1008 Arabidopsis Mediator subunit MED16 regulates iron homeostasis by associating
1009 with EIN3/EIL1 through subunit MED25. Plant J. **77**: 838–851.
1010 **Yuan, Y., Wu, H., Wang, N., Li, J., Zhao, W., Du, J., Wang, D., and Ling, H.Q.** (2008).
1011 FIT interacts with AtbHLH38 and AtbHLH39 in regulating iron uptake gene
1012 expression for iron homeostasis in Arabidopsis. Cell Res. **18**: 385–397.
1013 **Yuan, Y.X., Zhang, J., Wang, D.W., and Ling, H.Q.** (2005). AtbHLH29 of Arabidopsis
1014 thaliana is a functional ortholog of tomato FER involved in controlling iron
1015 acquisition in strategy I plants. Cell Res. **15**: 613–621.
1016 **Zhang, J., Liu, B., Li, M., Feng, D., Jin, H., Wang, P., Liu, J., Xiong, F., Wang, J., and**
1017 **Wang, H.** (2015). The bHLH Transcription Factor bHLH104 Interacts with IAA-
1018 LEUCINE RESISTANT3 and Modulates Iron Homeostasis in Arabidopsis. Plant Cell
1019 **27**: 787–805.
1020 **Zhang, Y., Wu, H., Wang, N., Fan, H., Chen, C., Cui, Y., Liu, H., and Ling, H.Q.**
1021 (2014). Mediator subunit 16 functions in the regulation of iron uptake gene
1022 expression in Arabidopsis. New Phytol. **203**: 770–783.
1023 **Zhu, P., Lister, C., and Dean, C.** (2021). Cold-induced Arabidopsis FRIGIDA nuclear
1024 condensates for FLC repression. Nature **599**: 657–661.
1025

Trofimov et. al. Figures and figure legends

Figure 1

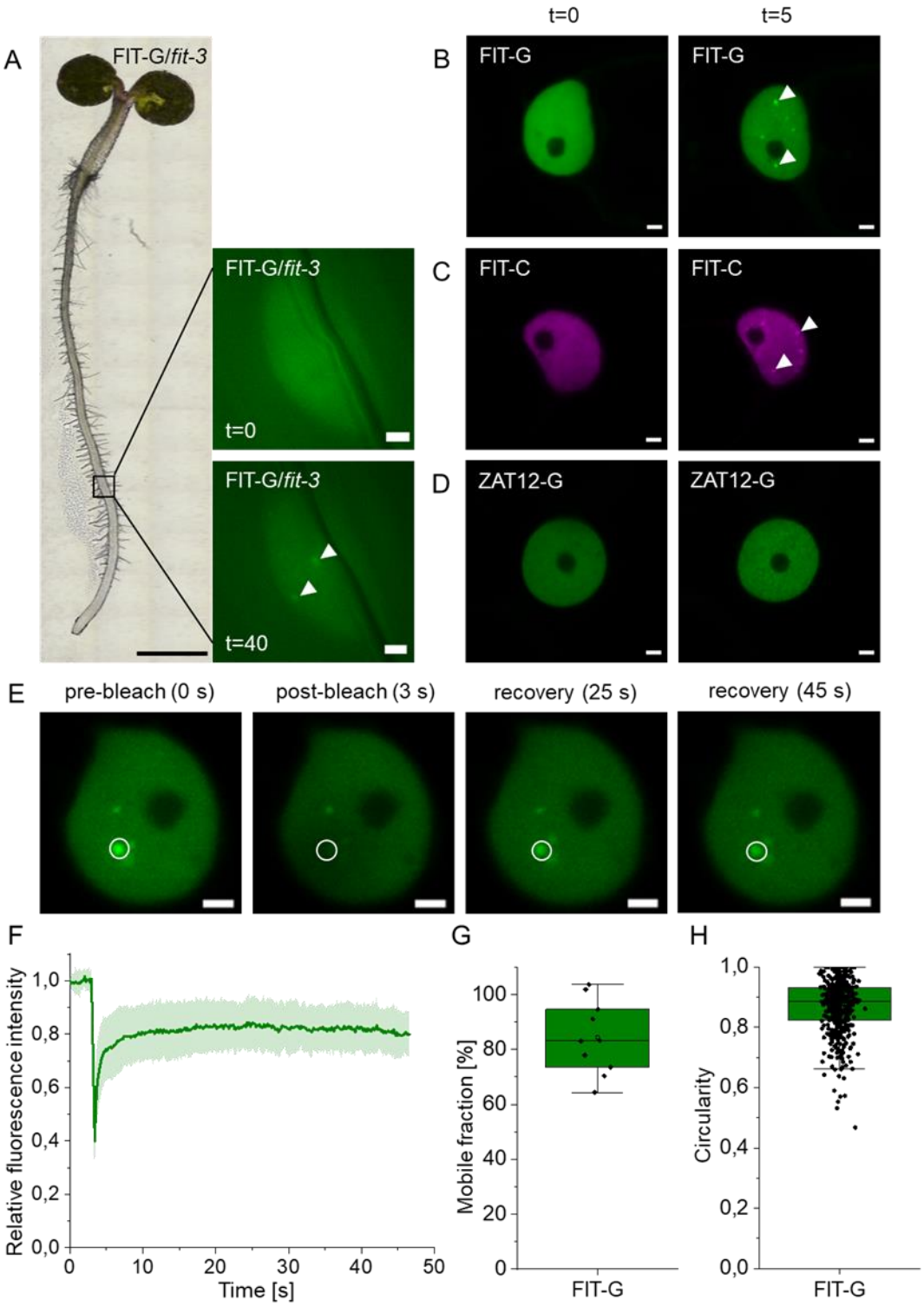

Figure 1: FIT accumulated in nuclear condensates, termed FIT nuclear bodies (NBs) in a light-inducible manner, most likely following liquid-liquid phase separation (LLPS).

A, Induction of FIT NBs in Arabidopsis root epidermis cells of the root differentiation zone. Left, light microscopy overview image of a 5-d-old Arabidopsis seedling (FIT-GFP/*fit-3*) grown in iron deficiency. Right, nuclear localization of FIT-GFP in the root epidermis cells as indicated in the overview image, at t=0 and t=40 min. FIT-GFP signals were evenly distributed in the nucleus at t=0 min, and after induction by excitation with 488 nm laser NB formation accumulated in NBs at t=40 min. Note that root epidermis cells developed few NBs with weak FIT-GFP signals, sometimes taking up to two hours to appear. Four independent experiments with three plants were conducted. In the indicated region of interest, approximately a quarter of the root epidermis cells showed NBs. A representative image from one nucleus is shown. B-D, Fluorescence protein analysis in transiently transformed *N. benthamiana* leaf epidermis cells. Confocal images of B, FIT-GFP, C, FIT-mCherry, and D, ZAT12-GFP at t=0 and t=5 min. At t=0 min, FIT-GFP and FIT-mCherry showed an even distribution within the nucleus. Following a 488 nm laser excitation, numerous NBs were clearly visible in all examined transformed cells at t=5 min. These NBs were termed FIT NBs. Under the same imaging conditions, ZAT12-GFP did not show NB formation. According to these results, a standardized FIT NB analysis procedure was set up (**Supplemental Figure S1**). See also **Supplemental Movie S1A-C**. Representative images from two to three independent experiments. E-G, FRAP measurements to test for liquid-like behaviour of FIT NBs, using the standardized FIT NB analysis procedure in transiently transformed *N. benthamiana* leaf epidermis cells. E, Representative images of the fluorescent signal during a FRAP experiment, taken before bleaching (0 s) and recovery of fluorescence at three time points after bleaching from 3 s to 45 s within the circled region of a NB. F, Line diagram representing the relative fluorescence during a FRAP measurement for 10 NBs, showing a high fluorescence recovery rate of FIT-GFP within NBs. Dark green line, mean value; light green filled area, variation. G, Box plot diagram representing the mobile fraction of FIT-GFP calculated based on the relative fluorescence recovery in F. The diagram indicates high mobility of FIT. The mean was calculated from 10 NBs from 10 nuclei from a transformed plant. Three independent experiments were conducted, one representative result is shown. H, Box plot diagram representing quantification of the FIT NB shape with the software ImageJ

(National Institutes of Health), indicating that FIT NBs have circular shape. Mobility and circularity characteristics indicate that FIT NBs are most likely liquid condensates that are the result of LLPS. The mean was calculated from all NBs visible in 15 nuclei from a transformed plant. Two independent experiments were conducted, one representative result is shown.

Box plots show 25-75 percentile with min-max whiskers, mean as small square and median as line. Scale bars of nuclei images, 2 µm; scale bar full seedling, 1 mm. Arrowheads indicate NBs. G = GFP; C = mCherry.

45 **Figure 2**

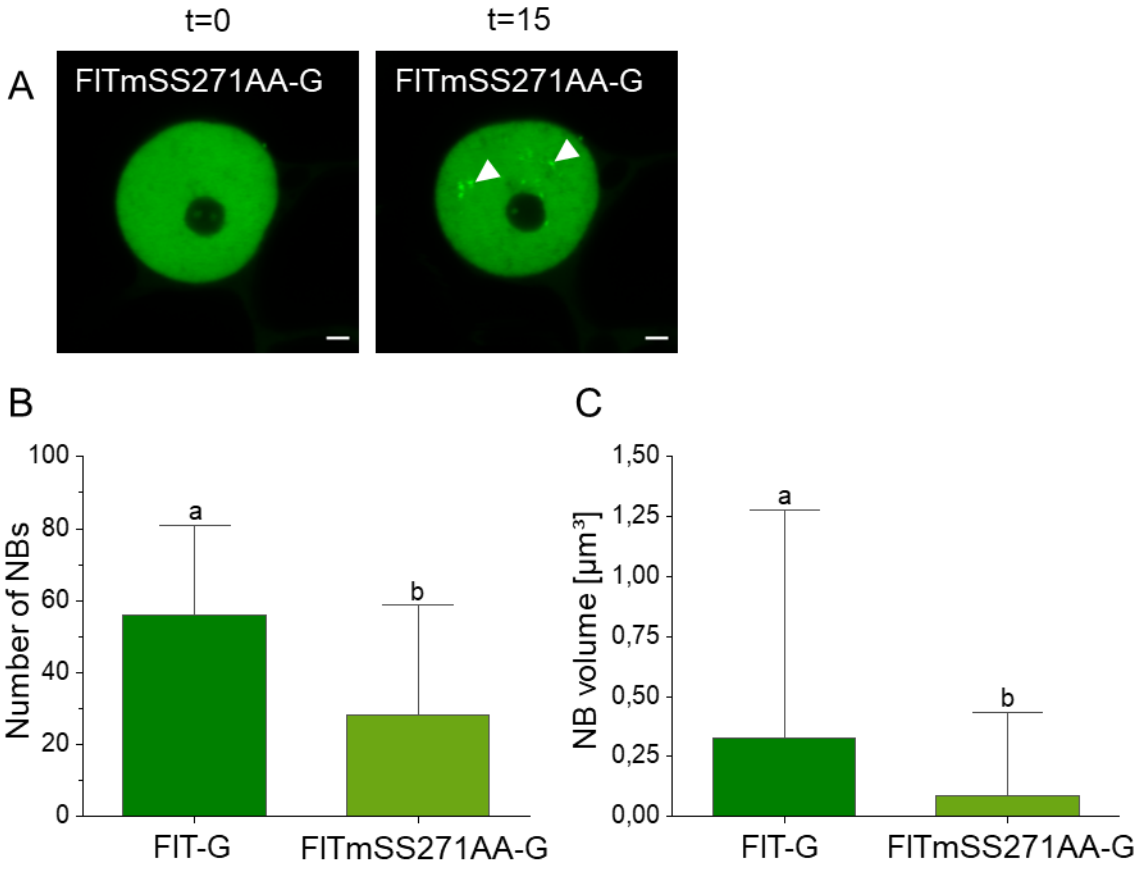

46

Figure 2: The FIT C-terminal Ser271/272 site was important for the capacity of FIT to localize to NBs.

A, Confocal images of nuclear localization of FITmSS271AA-GFP at t=0 and t=15 min. FITmSS271AA-GFP accumulated in NBs, but NB formation required a longer time compared to FIT-GFP. See also **Supplemental Movie S1, A and C**. Two independent experiments. Representative images from one nucleus. B, Bar diagrams showing in B, number of NBs, and in C, the sizes of NBs with FIT-GFP and FITmSS271AA-GFP at t=5/15 min. NB number and size were determined with the software ImageJ (National Institute of Health). FIT-GFP accumulated in more and larger NBs than FITmSS271AA-GFP. See **Supplemental Movie S1, A and C**. FITmSS271AA-GFP lacks IDR$^{Ser271/272}$. This IDR may be relevant for FIT NB formation (**Supplemental Figure S2**). In B and C, bar diagrams represent the mean and standard deviation for a quantification of 15 nuclei from a transformed plant (n = 15). Two experiments were conducted, one representative result is shown.

Statistical analysis was performed with the Mann-Whitney test. Different letters indicate statistically significant differences ($P < 0.05$). Scale bar: 2 µm. Arrowheads indicate NBs. G = GFP. Analysis was conducted in transiently transformed *N. benthamiana* leaf epidermis cells, following the standardized FIT NB analysis procedure.

66 **Figure 3**

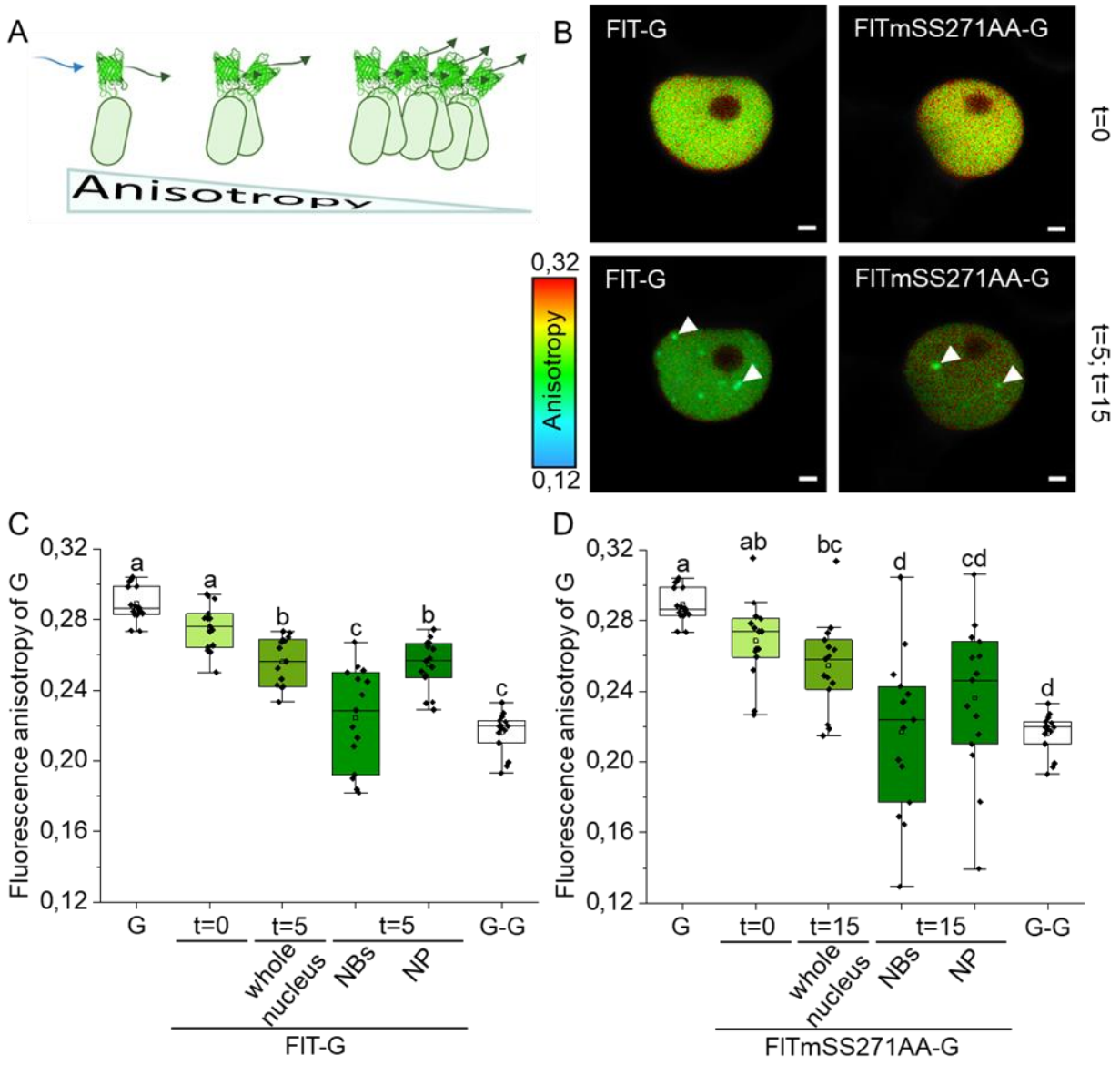

67

Figure 3: FIT was present in homodimeric protein complexes in NBs, dependent on Ser271/272 site.

Anisotropy (or homo-FRET) measurements of FIT-GFP and FITmSS271AA-GFP to determine homodimerization strength. A, Schematic illustration of the anisotropy principle. Energy transfer between the same kind of fluorescently tagged proteins leads to depolarization of the emitted light. Extent of the depolarization gives a hint on dimerization and oligomerization of a protein as the fluorescence anisotropy (FA) value decreases. B, Representative images showing colour-coded FA values of FIT-GFP and FITmSS271AA at t=0 and t=5/15 min. C-D, Box plots representing quantification of FA values. FA was measured at t=0 within the whole nucleus and at t =5/15 min within the whole nucleus, in NBs and in residual NP. Free GFP and GFP-GFP served as references for mono- and dimerization. FA values for C, FIT-GFP, and D, FITmSS271AA-GFP. In C and D, FA values were calculated from 10-15 nuclei from a transformed plant (n = 10-15). Two experiments were conducted, one representative result is shown. C and D show the same free GFP and GFP-GFP references because both measurements were performed on the same day. FA values decreased for FIT-GFP, but not FITmSS271AA-GFP, in the whole nucleus (compare t=0 with t=5/15 min). FA values were also lowered in NBs versus NP in the case of FIT-GFP but not FITmSS271AA-GFP (compare t=5/15 min of NBs and NP). This indicates stronger homodimerization of FIT than FITmSS271AA-GFP in the whole nucleus and in NBs. $IDR^{Ser271/272}$ may therefore be relevant for FIT NB formation and FIT homodimerization (**Supplemental Figure S2**).

Box plots show 25-75 percentile with min-max whiskers, mean as small square and median as line. Statistical analysis was performed with one-way ANOVA and Tukey post-hoc test. Different letters indicate statistically significant differences ($P < 0.05$). Scale bar: 2 µm. Arrowheads indicate NBs. G = GFP. Fluorescence protein analysis was conducted in transiently transformed *N. benthamiana* leaf epidermis cells, following the standardized FIT NB analysis procedure.

95 **Figure 4**

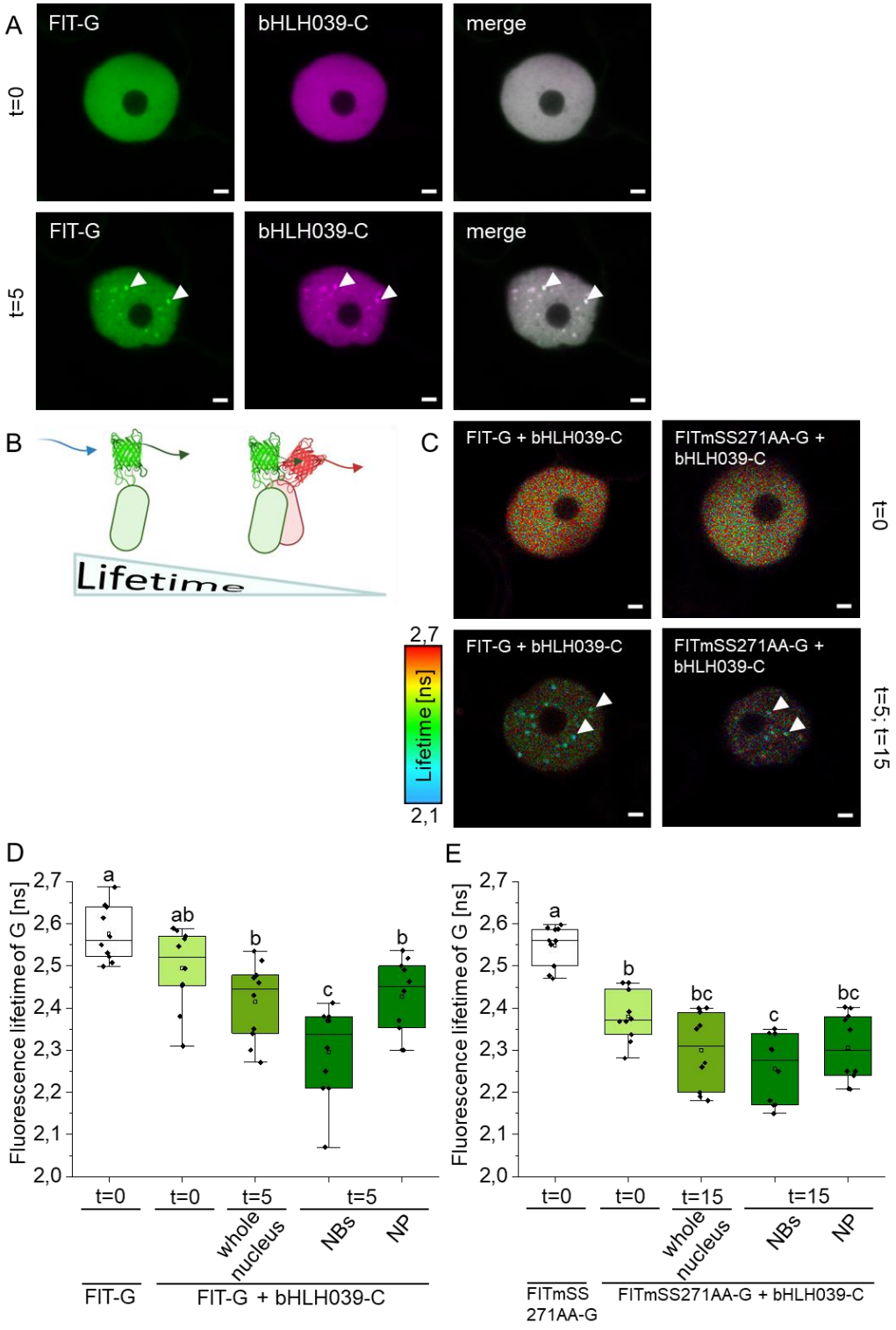

96

Figure 4: FIT was present in heterodimeric protein complexes with bHLH039 in NBs, dependent on Ser271/272 site.

A, Confocal images with colocalization of FIT-GFP and bHLH039-mCherry in the nucleus. Both proteins were evenly distributed within the nucleus at t=0 and colocalized fully in FIT NBs at t=5 min. Two independent experiments with two plants each. Representative images from one nucleus. B-E, FRET-FLIM measurements to determine heterodimerization strength of FIT and FITmSS271AA with bHLH039, respectively. FIT-GFP and FITmSS271AA-GFP (donor only) served as negative controls. B, Schematic illustration of the FRET-FLIM principle. Energy transfer occurs between two different fluorophores. One fluorophore acts as the donor and the other as the acceptor of the energy. In case of interaction (close proximity, ≤10 nm) the fluorescence lifetime of the donor decreases. C, Representative images showing colour-coded fluorescence lifetime values of FIT-GFP and FITmSS271AA-GFP co-expressed with bHLH039-mCherry at t=0 and t=5/15 min. D-E, Box plots diagrams representing FRET-FLIM measurements at t=0 within the whole nucleus and at t=5/15 min within the whole nucleus, inside NBs and in residual NP. Lifetime values represent measurements of 10 nuclei from a transformed plant (n = 10). Two experiments were conducted, one representative result is shown. Fluorescence lifetime was reduced for the pair of FIT-GFP and bHLH039-mCherry in NBs versus NP at t=5 min, indicating protein interaction preferentially inside NBs. Fluorescence lifetime values were not significantly different for the pair FITmSS271AA-GFP and bHLH039-mCherry in this same comparison at t=15 min, indicating that this pair did not preferentially interact in NBs. $IDR^{Ser271/272}$ may therefore be relevant for FIT NB formation, and FIT homo- and heterodimerization (**Supplemental Figure S2**).

Box plots show 25-75 percentile with min-max whiskers, mean as small square and median as line. Statistical analysis was performed with one-way ANOVA and Tukey post-hoc test. Different letters indicate statistically significant differences ($P < 0.05$). Scale bar: 2 µm. Arrowheads indicate NBs. G = GFP; C = mCherry. Fluorescence protein analysis was conducted in transiently transformed *N. benthamiana* leaf epidermis cells, following the standardized FIT NB analysis procedure.

Figure 5

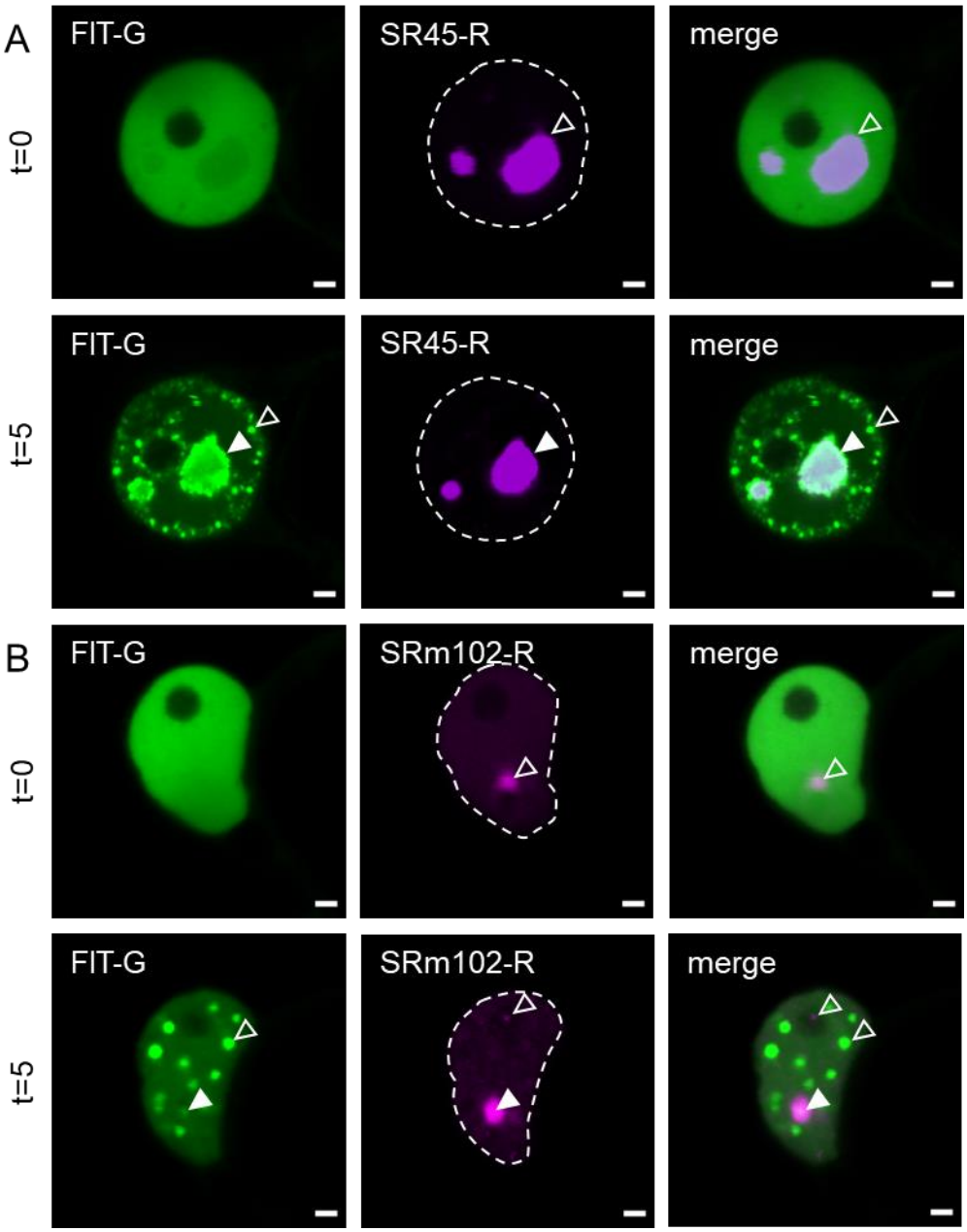

Figure 5: Two NB markers and splicing components were present in NBs in which FIT accumulated after the light trigger, whereas they were not part of FIT NBs (designated type II).

Confocal images showing localization of FIT-GFP and NB markers (type II) upon co-expression in the nucleus at t=0 and t=5 min. Co-expression of FIT-GFP with A, SR45-mRFP, and B, SRm102-mRFP. Type II NB markers localized inside NBs at t=0 and t=5 min. Similar localization patterns were observed upon single expression, showing that SR45 and SRm102 are present in distinct NB types (compare with **Supplemental Figure S4, A and B**). FIT-GFP colocalized with type II markers in their distinct NBs at t=5 min, but not t=0. FIT-GFP additionally localized in FIT NBs at t=5 min. Type II markers were not present in FIT NBs, while FIT-GFP became recruited into the distinct type II NBs upon the light trigger. Hence, FIT NBs could be associated with speckle components.

Scale bar: 2 µm. Filled arrowheads indicate colocalization in NBs, empty arrowheads indicate no colocalization in NBs. G = GFP; R = mRFP. Fluorescence protein analysis was conducted in transiently transformed *N. benthamiana* leaf epidermis cells, following the standardized FIT NB analysis procedure. Representative images from two to five independent experiments are shown. For data with type I markers (no colocalization) and type III markers (full colocalization) see **Supplemental Figure S3** and **Figure 6**.

147 **Figure 6**

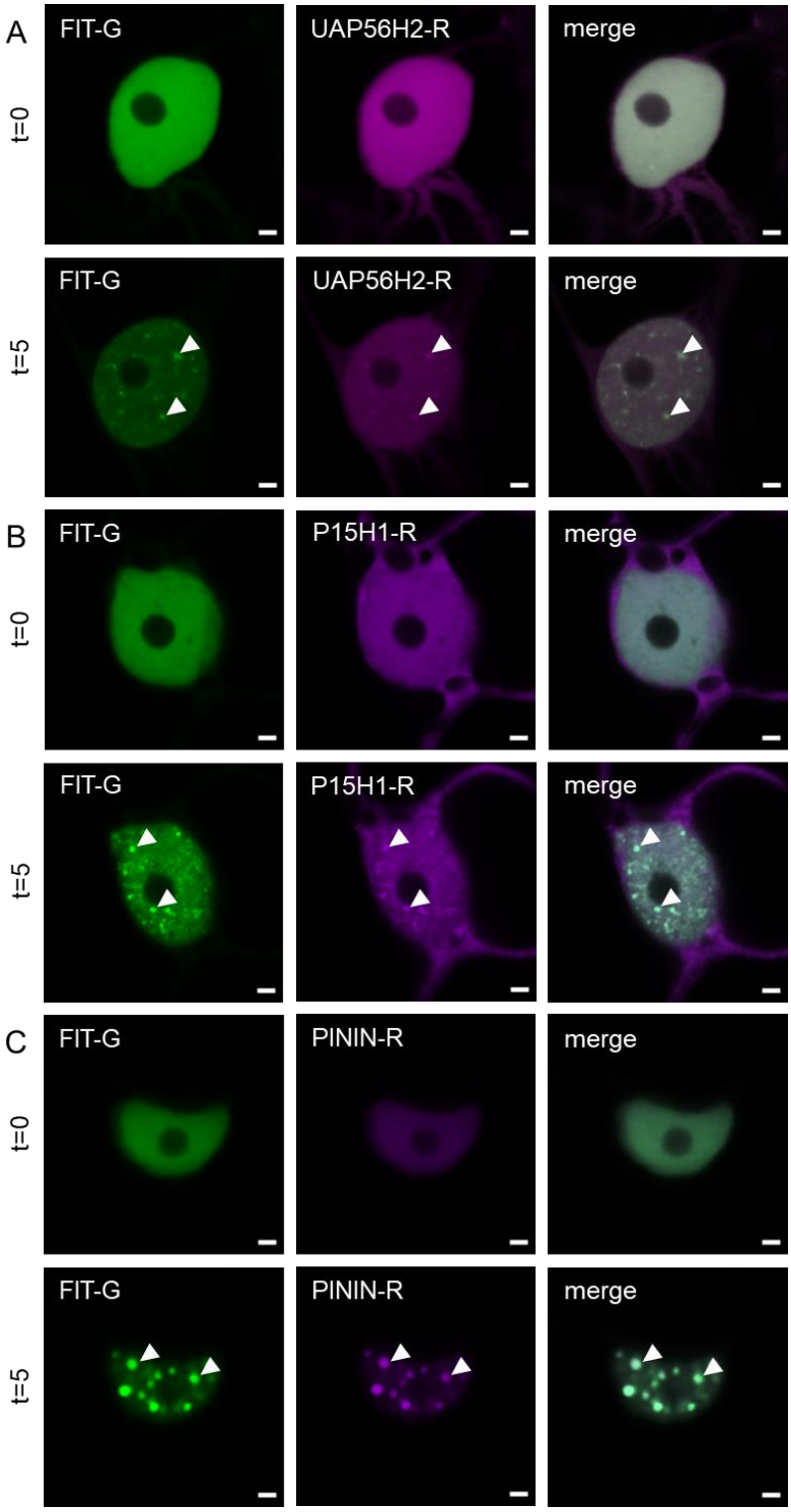

148

Figure 6: Three NB markers and speckle components became localized in FIT NBs and colocalized fully with FIT (designated type III), suggesting that FIT NBs have speckle function.

Confocal images showing localization of FIT-GFP and NB markers (type III) upon co-expression in the nucleus at t=0 and t=5 min. Co-expression of FIT-GFP with A, UAP56H2-mRFP, B, P15H1-mRFP, and C, PININ-mRFP. All three type III NB markers were homogeneously distributed and colocalized with FIT-GFP in the nucleus at t=0, while they colocalized with FIT-GFP in FIT NBs at t=5 min. UAP56H2-mRFP and P15H1-mRFP showed homogeneous localization in the single expression at both t=0 and t=5 min (compare with **Supplemental Figure S4, C and D**), while PININ-mRFP localized mainly in one large and several small NBs upon single expression at t=0 and t=5 min (compare with **Supplemental Figure S4E**). Hence, these three markers adopted the localization of FIT-GFP upon co-expression and suggest that FIT NBs have a speckle function.

Scale bar: 2 µm. Arrowheads indicate colocalization within NBs. G = GFP; R = mRFP. Fluorescence protein analysis was conducted in transiently transformed *N. benthamiana* leaf epidermis cells, following the standardized FIT NB analysis procedure. Representative images from four to seven independent experiments are shown. For data with type I markers (no colocalization) and type II markers (partial colocalization) see **Supplemental Figure S3** and **Figure 5**.

168 **Figure 7**

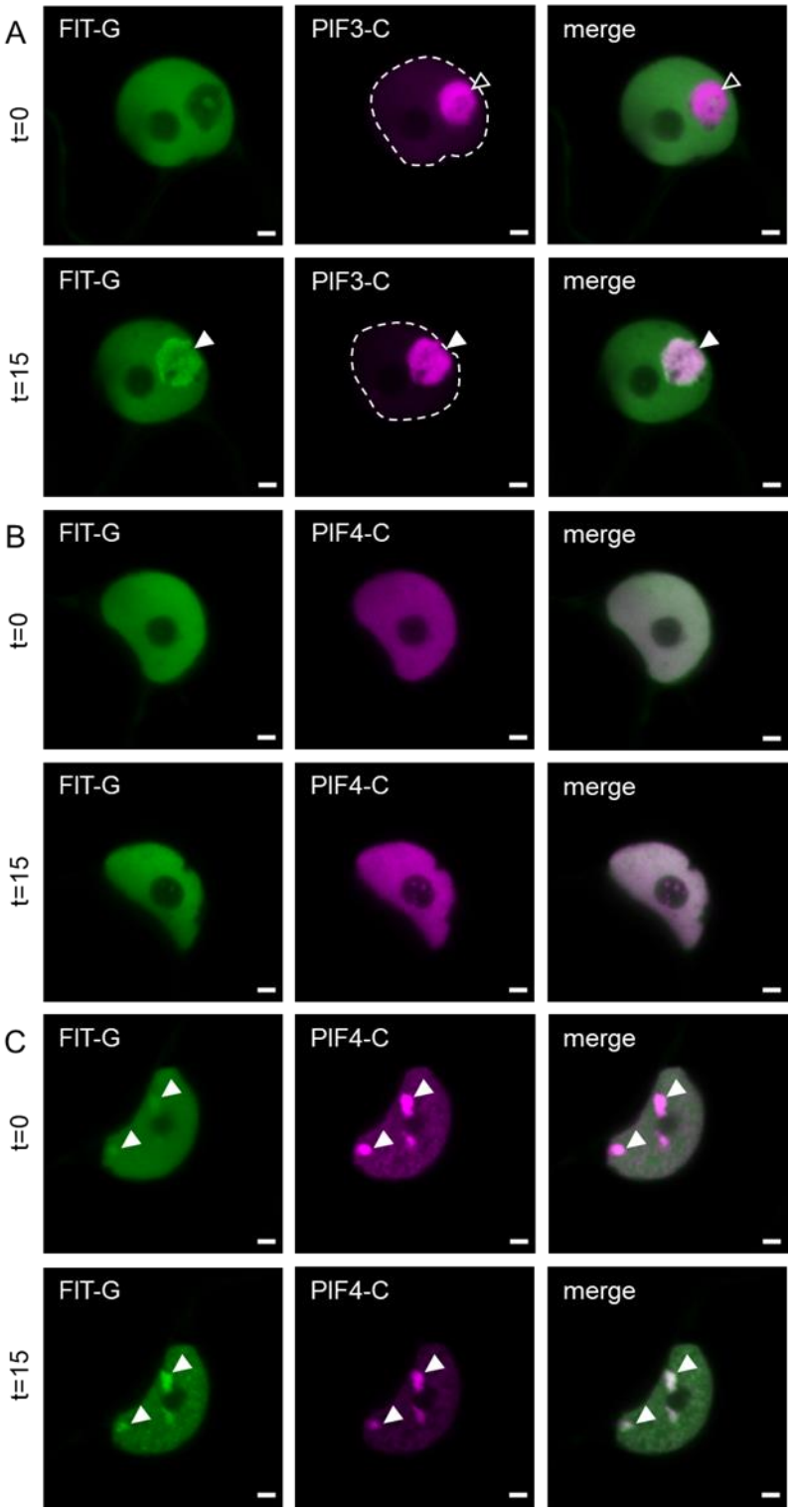

169

Figure 7: FIT colocalized with photobody (PB) markers in distinct PBs.

Confocal images showing localization of FIT-GFP and PB markers upon co-expression in the nucleus at t=0 and t=15 min. Co-expression of FIT-GFP with A, PIF3-mCherry, and B and C, PIF4-mCherry, in B, showing a typical pattern with absence of NBs (ca. 50% of nuclei), in C, showing a typical pattern with presence of NBs (ca. 50% of cells). When FIT-GFP was co-expressed with PB markers, FIT NBs did not appear at t=5 min, but instead, FIT-GFP colocalized with PB markers in PBs at t=15 min. A, PIF3-mCherry localized predominantly to a single large PB at t=0 and t=15 min. FIT-GFP colocalized with PIF3-mCherry in this single large PB at t=15 min. B, PIF4-mCherry and FIT-GFP were both homogeneously distributed in the nucleoplasm at t=0 and t=15 min. In C, FIT-GFP colocalized with PIF4-mCherry in PBs at t=0 and t=15 min. The same localization patterns were found for PIF3-mCherry and PIF4-mCherry upon single expression (compare with **Supplemental Figure S5**). Hence, FIT-GFP was recruited to the two distinct types of PIF3 and PIF4 PBs, whereas PIF3 and PIF4 were not recruited to FIT NBs. This suggests that FIT NBs are affected by the presence of PIF3- and PIF4-containing PBs and a connection to light signalling exists.

Scale bar: 2 µm. Arrowheads indicate colocalization in PBs. G = GFP; C = mCherry. Fluorescence protein analysis was conducted in transiently transformed *N. benthamiana* leaf epidermis cells, following the standardized FIT NB analysis procedure. Representative images from four to six independent experiments are shown.

Figure 8

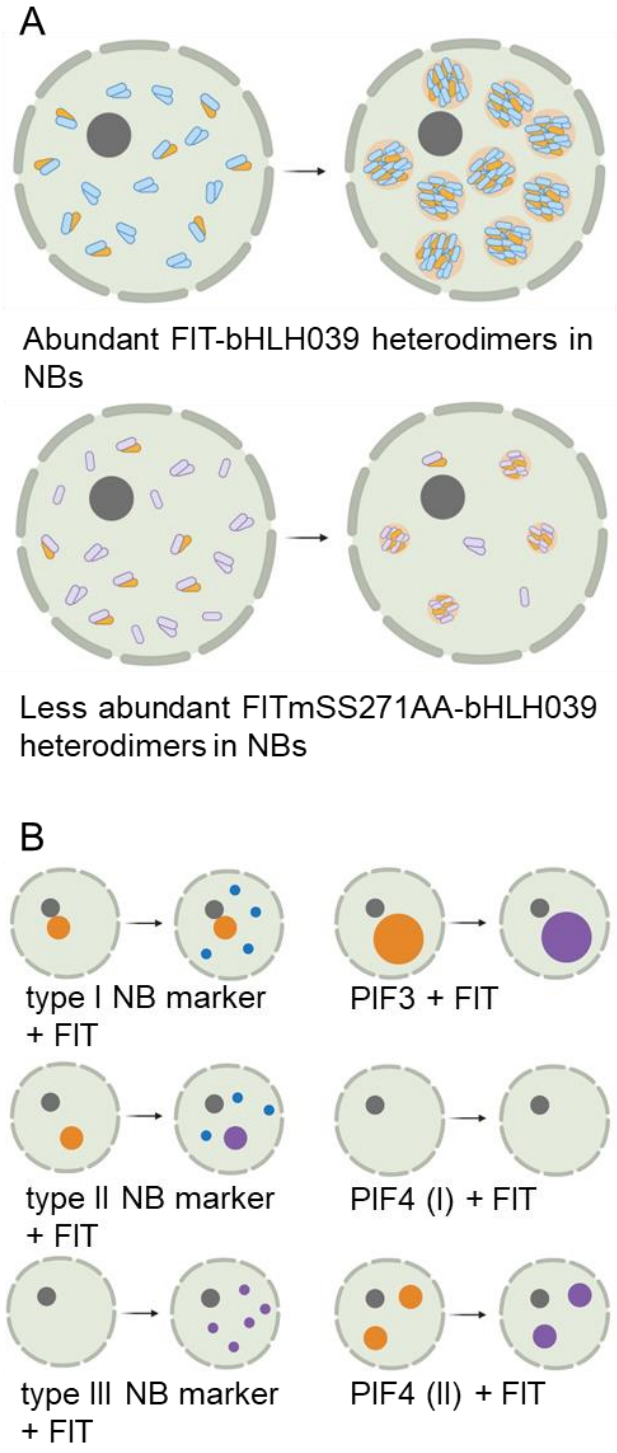

Figure 8: Schematic summary models illustrating the dynamics of FIT NB formation, suggesting that FIT NBs are related to transcriptional and posttranscriptional regulation in speckles.

A, Light-induced FIT NB formation in the presence of FIT (top) or FITmSS271AA (bottom) and bHLH039. FIT accumulates in FIT NBs, that are of circular shape and may undergo LLPS. FIT homodimers and FIT-bHLH039 heterodimers are present in the nucleus at t=0 and t=5 min. At t=5 min, homo- and heterodimers are preferentially present in FIT NBs versus NP. $IDR^{Ser271/272}$ may be important for multivalency of FIT, as it is disrupted in FITmSS271AA. This mutant has low protein interaction ability (see also Gratz et al., 2019). Consequently, FITmSS271AA accumulates slowly in NBs (taking up to t=15 min). FIT-bHLH039 is an active TF complex for upregulating the expression of iron acquisition genes in roots in contrast to FITmSS271AA-bHLH039 (Gratz et al., 2019). Hence, FIT NBs are subnuclear sites related to transcriptional regulation and because of their colocalization with speckle components, also to speckles. B, Dynamics of NBs revealed by co-expression. FIT did not colocalize with type I NB markers (Cajal body markers; coilin, U2B''). FIT colocalized with type III markers (speckle components; UAP56H2, P15H1, PININ) and these markers adopted the FIT pattern at t=5 min following the light trigger. Type II NB markers (speckle components; SR45, SRm102) and PB markers (PIF3, PIF4) localized to their own distinct NBs into which FIT became recruited in light-inducible manner. In case of type II NB markers, these markers did not localize in FIT NBs. Hence, there is a light-inducible effect acting upon FIT to become recruited by type II NBs and PBs or to recruit proteins into its own NBs. In summary, FIT NBs are light-inducible subnuclear sites linking transcriptional and posttranscriptional regulation in speckles.

A, Blue ovals = wild-type FIT; violet ovals = mutant FITmSS271AA; orange ovals = bHLH039. B, grey circles = nucleoli; orange circles = NB/PB marker NBs/PBs; blue circles = FIT NBs; lilac circles = colocalization of NB/PB marker NBs/PBs and FIT NBs.